Bull. Chem. Soc. Jpn., 72, 179—197 (1999)

Structural Genealogy of BEDT-TTF-Based Organic Conductors II. Inclined Molecules: θ, α, and $\varkappa$ Phases

Takehiko Mori,* Hatsumi Mori,† and Shoji Tanaka†

Department of Organic and Polymeric Materials, Tokyo Institute of Technology, O-okayama, Tokyo 152-8552

†International Superconductivity Technology Center, Shinonome, Tokyo 135-0062

(Received July 7, 1998)

Overlap integrals between HOMO's of two non-parallel BEDT-TTF (bis(ethylenedithio)tetrathiafulvalene) molecules have been calculated. As the dihedral angle between the molecular planes decreases from 180° (parallel) to 90° (perpendicular), the overlap integral increases and attains a maximum around 90°. This accounts for the "universal phase diagram" of the θ-phase; θ-salts vary from an insulator to a metal with decreasing the dihedral angle. The ratio of the lattice constants in the conducting plane, c/a, changes in proportion to the dihedral angle. Thus c/a can be used instead of the dihedral angle. A similar universal phase diagram is applicable to analogous phases like α and α'', and also to the corresponding phases of other donors. The properties of $\varkappa$-phase salts are similarly scaled by c/a. As c/a increases, the intradimer overlap integral decreases owing to the increase of the intradimer spacing, and correlated insulator, superconductor, and simple-metal phases appear in succession. When c/a increases further, another insulating phase emerges due to the decrease of the interdimer overlaps. Chemical pressure in both θ- and $\varkappa$-phases reduces c/a, and stabilizes the insulating state. Hydrostatic physical pressure gives the same influence in the θ-phase, but enhances the interdimer interaction in the $\varkappa$-phase to result in the opposite effect. A diagram is proposed to illustrate which structures of β, β'', θ, and $\varkappa$ are favored by BEDT-TTF and other donors.

In the preceding report, we have investigated geometry dependence of overlap integrals between HOMO's of two BEDT-TTF (or ET for short) molecules for the geometries in which both the molecular planes and the molecular long axes are parallel to each other.[1,2] Based on this analysis, we have discussed classification of various modifications of β and β''-phase salts. In the present work, we will study the overlap integrals of inclined ET molecules, where the molecular long axes are still parallel to each other but the molecular planes are not parallel any more. This kind of inclined interaction appears in θ, α, and $\varkappa$-phases; the principal purpose of the present report is to provide a universal perspective on the relations of structure and physical properties in these phases. There is another type of frequently observed molecular arrangement, twisted dimer structure, where the molecular long axes are not parallel but the molecular planes are parallel to each other. This structure appears in $\delta(\beta\text{-PF}_6)$ and α'-phases. These phases will be discussed in a succeeding paper.[3]

Fermi surfaces of ET-based conductors have been predicted from a simple calculation where the transfer integrals are estimated from overlap of HOMO's, and the band structure is calculated on the basis of the tight-binding approximation. In these calculations, isostructural salts afford a similar set of transfer integrals with approximately the same Fermi surface. As a consequence, salts of the same structure usually exhibit similar physical properties. However, θ-phase salts show a wide variety of properties from an insulator to a superconductor; this has been a great mystery for a long time.

Recently we have prepared a series of new θ-phases, θ-$(ET)_2MM'(SCN)_4$ by changing the metal atoms, M = Cs, Rb, and Tl, and M′ = Co and Zn.[4—7] We have found that the metal-insulator (M-I) transition temperature T_{MI} changes as a function of the dihedral angle between the molecular planes.[8,9] It has been also discovered that the bandwidth W of θ-phase increases with a decrease of the dihedral angle. Accordingly all θ-phase salts are located on a single phase diagram, where the dihedral angle is taken as the horizontal axis. This finding has prompted us to explore geometry dependence of the overlap integrals for inclined ET molecules.

In this paper, we will investigate the inclination angle dependence of the overlap integrals. The results will be applied to θ and α-phases, to account for a universal phase diagram that is applicable to many salts of the same structure type. Along with the dihedral angle, the ratio of the lattice constants, c/a is a good parameter which determines the bandwidth. A similar analysis will be applied to $\varkappa$-phase, and we will attempt to extend Kanoda's phase diagram to all $\varkappa$-phases.[10] In the present paper we will provide lists of all reported θ, α, and $\varkappa$-salts of ET, BO, and BETS (BO: bis(ethylenedioxy)tetrathiafulvalene, BETS: bis(ethylenedithio)tetraselenafulvalene) (Scheme 1).

θ-Phase

Molecular Coodinates of Inclined Molecules. The donor arrangement of a θ-phase salt viewed along the molecular long axis is depicted in Fig. 1. A θ-phase is composed

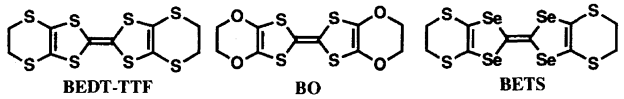

Scheme 1.

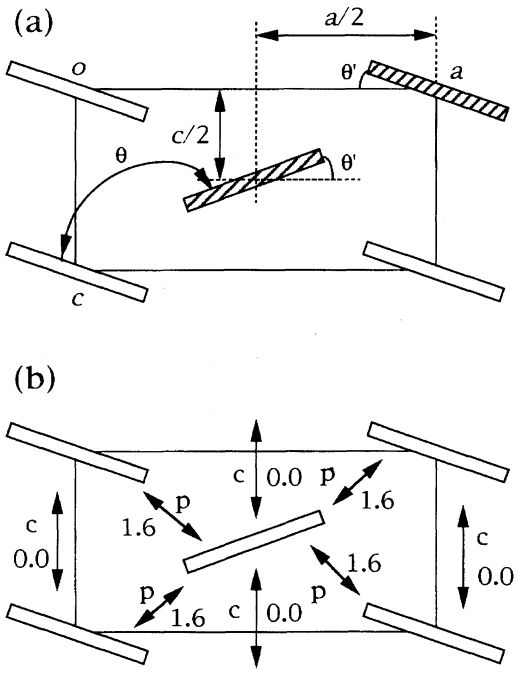

Fig. 1. (a) Donor arrangement of a θ-phase salt viewed along the molecular long axis, and (b) displacement along the molecular long axis, D/Å in θ-$(ET)_2CsCo(SCN)_4$.

of so-called herring-bone type donor arrangements. Stacks of the θ-phases are made up of the ring-over-atom (RA) overlap mode,[1] and the adjacent pseudo-stacks are inclined toward opposite directions (Figs. 5 and 6 in Ref. 1). Following the choice of crystal axes in θ-$(ET)_2MM'(SCN)_4$,[4] we shall define the direction of the pseudo-stacking as the c axis, and the transverse direction in the conducting sheet as the a axis. The molecular long axes are parallel to the crystallographic b axis. Similarly to two parallel ET molecules, the displacement along the molecular long axis for each pair of adjacent ET molecules will be referred to as D. The D values of θ-$(ET)_2CsCo(SCN)_4$ are shown in Fig. 1(b).

The distinction between θ- and α-phases is sometimes obscure. The θ-phases listed in Table 1 are uniform along the pseudo-stacking (c) axis, but have two-fold periodicity along the b axis (the notation of the crystal axes is shown in Fig. 1(a)). We shall designate this as (c, $2b$). These θ-phases have orthorhombic or monoclinic symmetry. By contrast, the prototype α-$(ET)_2I_3$ has ($2c$, b) periodicity. The phases usually designated as α-phase have triclinic symmetry. The structure of the prototype θ-$(ET)_2I_3$ has been first reported as (c, $2b$) and orthorhombic, but this salt has $2c$ periodicity originating in the anion lattice, so that the actual periodicity is ($2c$, $2b$) with monoclinic symmetry.[15] In the present work, we shall designate any phases with uniform c donor arrangement as θ-phase (including θ-$(ET)_2I_3$), and those with $2c$ lattice as α-phase. This corresponds to the difference of the Fermi surface; the former has a large connected one, and the latter has a gap between separated parts.

θ-Phase has only two kinds of intermolecular interactions, c and p (Fig. 1(b)). In the c interaction, the two molecules are parallel to each other; so this interaction is able to be understood in the context of Ref. 1. This interaction is oriented to the ϕ = ca. 60° direction with respect to the molecular

Table 1. Lattice parameters of θ-Phase ET, BO, and BETS Salts

Compounds	a/Å	b/Å	c/Å	c/a	θ/°	T_{MI}/K	Z/L[a]	Ref.
$(ET)Ag_{2.4}Br_3$	11.699	40.287	4.232	0.362	132	> 300	L	11
$(ET)_2Cu_2(CN)[N(CN)_2]_2$	11.088	38.837	4.201	0.363	130	> 300	Z	12
$(ET)Ag_{1.6}(SCN)_2$	11.588	40.18	4.257	0.367	130	> 300	L	13
$(ET)Cd_{0.66}(SCN)_2$	11.542	41.469	4.277	0.371	128	> 300	L	5
θ-$(ET)_2Ag(CN)_2$(monocli.)	10.996	34.093	4.281	0.389	125	100?[b]	L	14
$(ET)_2TlZn(SCN)_4$	11.003	41.429	4.400	0.400	121	> 300	L	8
$(ET)_2TlCo(SCN)_4$	10.393	43.16	4.495	0.432	116	250	Z	8
$(ET)_2RbZn(SCN)_4$	10.175	43.301	4.647	0.457	111	190	Z	5
$(ET)_2RbCo(SCN)_4$	10.176	43.258	4.650	0.457	111	190	Z	5
$(ET)_2CsZn(SCN)_4$	9.816	43.443	4.870	0.496	105	20	Z	4
$(Et)_2CsCo(SCN)_4$	9.804	43.416	4.873	0.490	104	20	Z	4
θ-$(ET)_2I_3$	10.076	33.853	4.964	0.493	99	None	L	15
θ-$(ET)_2Ag(CN)_2$ (ortho.)	9.519	33.927	4.952	0.520	101	(15)	Z	14
$(ET)_4[C(CN)_2CONH_2]CuCl_2$	9.320	34.114	5.099	0.547	98	?	Z	16
$(ET)_4[C(CN)_2CONH_2]CuBr_2$	9.338	34.175	5.124	0.549	98	?	Z	16
$(BO)_2Cl(H_2O)_x$	8.593	16.27	5.108	0.594	92	None	L	17
θ-$(BETS)_2TaF_6$	11.596	37.93	4.240	0.366		25	L	18
$(BETS)_2PF_6$	11.595	36.850	4.259	0.368		28	L	19
$(BETS)_2AuI_2$	10.200	17.292	4.965	0.487		None	L	19
$(BETS)_2Ag(CN)_2$	9.5839	34.645	4.983	0.520		None	Z	20

a) Z: Z-mode, and L: L-mode in Fig. 6. b) Suspicious because determined only by ESR measurement.

plane, and is regarded as the ordinary RA interaction; this overlap mode corresponds to a maximum of the overlap integral. Similarly to other RA overlap modes, the displacement D is approximately zero. The overlap integral at $\phi = 60°$ is, however, smaller than the other interactions such as the ordinary ($\phi = 90°$) ring-over-bond (RB) overlap mode.

In the p interaction, however, the two molecular planes are not parallel any more, so we need a new treatment. To discuss the p interaction, we shall concentrate our attention on the two hatched molecules in Fig. 1(a), because the four p interactions in a unit cell are the same by the symmetry. Since the molecules are placed on two-fold axes running parallel to the b axis, *the positions of the molecular long axes are related to halves of the lattice constants, a/2 and c/2, as shown in Fig. 1(a).* The dihedral angle θ between the molecular planes is related to the inclination θ' as $\theta = 180° - 2\theta'$.

Dihedral Angle and the Lattice Constants. Lattice constants of θ-phase salts reported so far are listed in Table 1. The notation of the crystal axes have been transformed following θ-$(ET)_2CsCo(SCN)_4$. As the dihedral angle θ decreases (going down in Table 1), a decreases and c increases. Then in our calculation, when θ is changed, we have to change the position of the molecules at the same time. In actual crystals, *a, c and c/a are closely related to θ, as plotted in Fig. 2.* Least-squares fitting to Fig. 2(a) gives the following equation:

$$\theta = 205.062 - 205.34\, c/a. \quad (1)$$

By using this relation, we can estimate the dihedral angle θ (/° with the standard deviation of 1.4°) from the axis ratio c/a without knowing the atomic coordinates. Each lattice constant is obtained from the following equations (Fig. 2(b)):

$$a = 8.8861 - 4.0327\cos\theta,$$
$$c = 5.2277 + 1.5591\cos\theta, \quad (2)$$

with the standard deviations 0.238 and 0.035 Å respectively. In our model calculation, together with θ, we have changed the positions of the molecules so as to fulfill these relations.

Angle Dependence of Overlap Integral. The overlap integrals calculated as a function of θ, are depicted in Fig. 3. The method of calculation is the same as that described in Ref. 1. Since the p interaction of θ-phase always appears at $D = 1.6$ Å (Fig. 1(b)), the D value is fixed at 1.6 Å.

At $\theta = 180°$, the overlap takes a small value. This configuration corresponds to $\phi = 16°$ in the parallel molecules (Fig. 2(a) of Ref. 1), and is close to the point where the overlap crosses zero. As θ decreases, the overlap slightly decreases, makes a broad minimum around 140°, increases significantly below 140°, and attains a maximum around 80°. The actual θ-phase takes an angle between 100° and 130° (Fig. 2), so that in this region *the overlap rapidly increases with inecreasing θ.*

Figure 4 shows another model calculation. While one places two ET molecules on the same plane, and keeps the S–S distance constant (3.4 Å), the two ET molecules are rotated in the opposite directions around their inner S–S lines

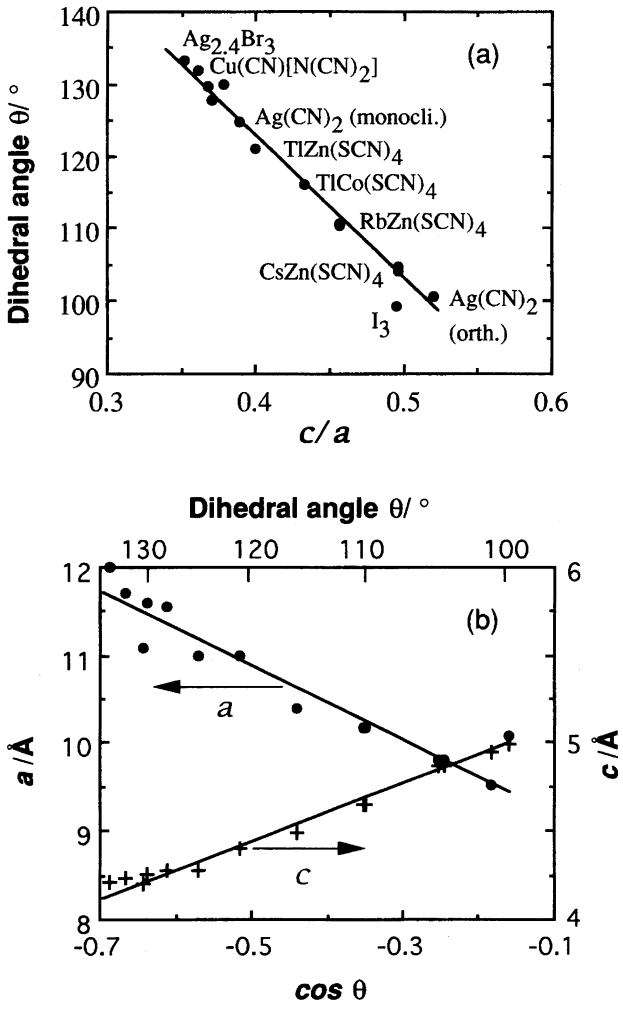

Fig. 2. Relation of lattice constants a and c to the dihedral angle θ in various θ-phase salts.

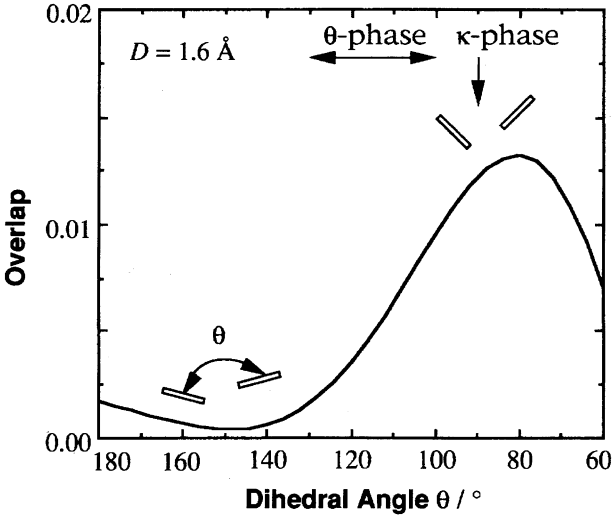

Fig. 3. Overlap integral of two inclined ET molecules as a function of the dihedral angle, θ. The positions of the molecules are moved according to the change of the lattice constants in the actual θ-phases (Fig. 2(b) and Eq. 2).

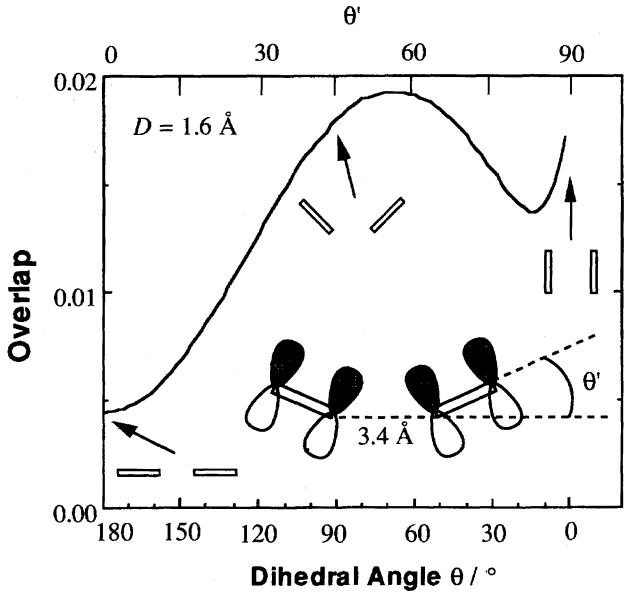

Fig. 4. Overlap integrals of two inclined ET molecules on the same horizontal level, as a function of the dihedral angle, θ for D = 1.6 Å.

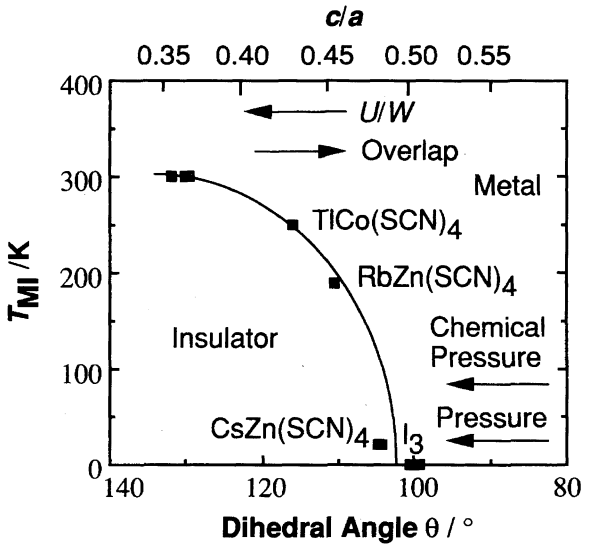

Fig. 5. Universal phase diagram of the θ-phase.

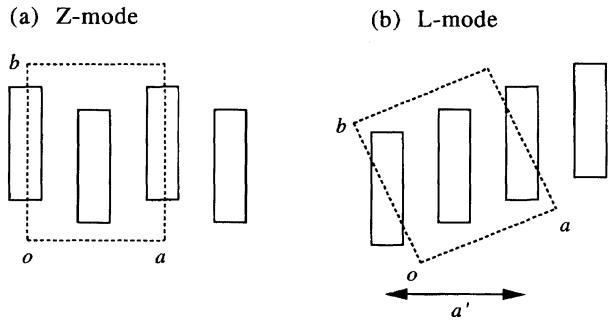

Fig. 6. Arrangements of pseudo-stacks in θ-phases, viewed along the stacking direction. (a) Z-mode and (b) L-mode.

running parallel to the molecular long axes. As the dihedral angle θ decreases, the overlap increases. This is convincing because, as shown in the inset, the comparatively weak side-by-side (π-like) overlap of the π-orbitals at $\theta = 180°$ is replaced by the direct (σ-like) overlap of the shaded lobes. The overlap integral monotonously increases from $\theta = 180°$ to 90° and attains a maximum around 80°. At $\theta = 90°$ the two molecules are perpendicular to each other. At $\theta = 0°$ the structure corresponds to the face-to-face stacking (the ring-over-bond (RB) mode). It is noteworthy that the oblique interaction around $\theta = 90°$ is as large as the face-to-face interaction. The situation of this calculation is not strictly the same as the actual interaction in the θ-phase, where the two molecules are shifted in the direction perpendicular to the molecular plane. Yet this calculation gives basically the same tendency as Fig. 4, and more clearly demonstrates that *the θ dependence of the overlap arises from the direct overlap of the π-lobes.*

Universal Phase Diagram. We shall also mention how the c interaction changes according to the change of θ. The angle ϕ in the interaction c is related to θ as $\phi = \theta/2$. When θ changes from 100° to 130°, ϕ changes 50° to 65°. As shown in Fig. 2 of Ref. 1, in this angle region the overlap once increases from a nearly zero value to a maximum at $\phi = 58°$ ($\theta = 116°$), and again decreases to zero towards $\theta = 130°$. Then the c interaction will be important near $\theta = 116°$. $(ET)_2TlCo(SCN)_4$ is located at this maximum ($\theta = 116°$), where c is 4.8×10^{-3} and p is 10.0×10^{-3}.[8] Even in this region, c is half of p. In a more typical case, for example in $(ET)_2CsCo(SCN)_4$ ($\theta = 104°$), p is -10.6×10^{-3} and c is 0.5×10^{-3}.[5]

The energy bands of θ-phase can be represented by a simple analytic form:[15]

$$E(k_a, k_c) = 2t_c \cos(k_c c) \pm 4t_p \cos(k_a a/2)\cos(k_c c/2). \quad (3)$$

Because θ-phase contains only two kinds of transfer integrals, and the energy dispersion relation is exceptionally simple, the values of not only t_p but also t_c have been estimated from the experiments of reflectance spectra ($t_p = 0.080$ eV and $t_c = 0.046$ eV for θ-$(ET)_2I_3$), and have been directly compared with the values obtained from the calculations.[21]

The p interaction is more important than the c interaction. According to the Eq. 3 above, the bandwidth W is equal to $8|t_p|$ as far as $t_c < |t_p|$, because both the top and the bottom of the energy bands come to the Γ point ($k_a = k_c = 0$). In fact, p appears twice as many times as c in a unit cell. Therefore *the p interaction has the primary importance in determining the bandwidth.*

From this, W must be a sensitive function of θ. When θ is large ($120° < \theta < 130°$), the small overlap (about $S = 0.0018$ in Fig. 3) leads to a very narrow band of 0.15 eV (obtained from $W = 8t_p$ and t = ES, where $E = -10$ eV).[1,2] On the other hand, the on-site Coulomb repulsion U is unchanged for a given donor molecule in any crystal structure. Consequently U/W becomes larger, and the correlation becomes stronger.

In Fig. 5, M-I transition temperatures T_{MI} of θ-salts are

plotted as a function of the dihedral angle θ. Many θ-salts with large dihedral angles ($\theta > 125°$) are paramagnetic insulators even at room temperature. As shown in the above model calculations, θ is related to W, so that the abscissa of Fig. 5 may be read as (decreasing) U/W. In the intermediate θ (105—120°), the system undergoes a transition from a high-temperature metal state to a low-temperature paramagnetic insulator. These M-I transitions have been observed below room temperature in three-component salts $(ET)_2MM'(SCN)_4$.

It should be noted that the insulator phases of the actual θ-phases are not simple Mott insulators. For instance, the 190 K M-I transition of $(ET)_2RbCo(SCN)_4$ is accompanied by the lattice dimerization along the c axis.[9] In this compound there is another transition to a spin singlet state at 20 K, but this singlet state appears only when the cooling rate is sufficiently slow. Furthermore the 20 K M-I transition of $(ET)_2CsZn(SCN)_4$ has an entirely different nature, and is purely paramagnetic. It is, however, obvious that *the bandwidth is regulated by the dihedral angle, and the decrease of the bandwidth makes the system susceptible to some kind of instability*. In the present work we shall not deal in detail with what kind of instability emerges in each salt, but only with how the bandwidth is controlled by the change of the structure.

When θ is still small ($< 102°$), the system remains metal down to low temperatures. This has been found in only two salts: θ-$(ET)_2I_3$ and orthorhombic θ-$(ET)_2Ag(CN)_2$. Superconductivity (3.6 K at ambient pressure) has been reported in the former salt,[15] but a slight increase of resistivity (20%) below 15 K has been reported in the latter salt.[14] In this θ region, the overlap (about 0.01) in Fig. 3 leads to $W = 0.8$ eV.[1,2] From the reflectance spectra, $8t_p$ in θ-$(ET)_2I_3$ has been estimated to be 0.64 eV.[21] It should be noted that within the usual range of θ ($100° < \theta < 130°$), W shows a remarkable change from 0.15 to 0.8 eV.

In Table 1, the entries are aligned in the increasing order of the axis ratio, c/a. The axis ratio has some advantage over the dihedral angle, because the atomic coordinates are not necessary to estimate it. *The M-I transition temperature drops to zero at a critical axis ratio of $c/a = 0.50$, or equivalently at $\theta = 102°$.*

BO and BETS. Lattice constants of BO and BETS-based θ-phase salts are listed in Table 1 as well. Because BO and BETS have the same symmetry of HOMO as that of ET, salts of these donors are expected to follow the same tendency. $(BO)_2Cl(H_2O)_x$ is the only BO-based θ-phase.[17] This salt has a particularly large c/a value (0.594) and a small dihedral angle (92°); this is in agreement with its metallic nature.

Among BETS salts, the TaF_6 and PF_6 salts with $c/a = 0.366$—0.368 undergo transitions around 25 K. In the ET salts, this transition temperature corresponds to $c/a = 0.490$—0.496 (approximately those of the CsZn and CsCo salts). From this, if we shift the horizontal axis of Fig. 5 by about $\Delta c/a = -0.12$, we can apply the same phase diagram to the BETS salts. In Table 2 are listed the critical values of c/a which gives $T_{MI} = 0$ K, and shifts of c/a with respect to the ET-based θ-phases.

Table 2. Critical Axis Ratio c/a ($T_{MI} = 0$ K) and Shift $\Delta c/a$ (in Parentheses) in the Universal Phase Diagrams

	θ	α	α''
ET	0.50	0.45 (−0.05)	0.55 (+0.05)
BO	<0.58 (<0.08)[a]	—[b]	0.45 (−0.05)[a]
BETS	0.38 (−0.12)	0.44 (−0.06)	—[b]

a) Not sufficiently many examples. b) No example.

Z-Mode and L-Mode. The D values of θ-phase are shown in Fig. 1(b). Along the transverse direction, namely as for the p interaction, D is 1.6 Å. When this displacement occurs alternately in the opposite directions along the a axis as $+-+-\cdots$, the pseudo-stacks are arranged as in Fig. 6(a). On the contrary, when all slips are aligned in the same direction like $++++\cdots$, a pattern such as that shown in Fig. 6(b) appears. We shall designate these two patterns as "Z-mode" and "L-mode", respectively.[22]

In the β and β'' phases, crystals except for those with $\times 2$ subscripts show L-mode pattern.[22] Yet, for example the $\beta''_{10\times2}$-phases such as $\beta''_{10\times2}$-$(BO)_2AuBr_2$ take the Z-mode arrangement; this is rather the origin of the transverse two-fold periodicity.

In the θ-phases, however, both arrangements appear almost with 1 : 1 probability. Table 1 lists these transverse arrangements. The Z-mode gives rise to a rectangular lattice (in the bc plane), because this pattern has a two-fold axis along the molecular long axis, or equivalently along the crystallographic b axis. Since the ac plane of a θ-phase is also rectangular, the Z-mode results in an orthorhombic lattice. By contrast, the L-mode brings about an oblique bc plane, leading to a monoclinic lattice. *All θ-phases with a monoclinic lattice have the L-mode.* Among the orthorhombic θ-phases $(ET)Ag_{2.4}Br_3$, $(ET)Ag_{1.6}(SCN)_2$, and θ-$(ET)_2I_3$ also have the L-mode, because the space groups of these phases do not have a two-fold axis along the molecular long axis. The Z-mode is realized if the phase satisfies the following two conditions: (1) it has an orthorhombic lattice, and (2) it has a two-fold axis along the molecular long axis (crystallographic b axis, which is usually the longest axis).

Two kinds of θ-$(ET)_2Ag(CN)_2$, with entirely the same composition, have been reported; these are distinguished as monoclinic and orthorhombic in the literature (Table 1).[14] The only difference of these salts are the L-mode and Z-mode arrangements of the donor chains.

In both Z-mode and L-mode arrangements, the D values are the same for all p interactions, and magnitudes of all p interactions are the same. Hence this difference exerts no influence on the energy band structure.

Strictly speaking, in the L-mode crystals, the distance designated as $a/2$ in Fig. 1(a) should be modified to $a'/2$ following the relation.

$$(a'/2)^2 = (a/2)^2 - (1.6\ \text{Å})^2. \quad (4)$$

Then we should compare c/a' instead of c/a in Table 1 and Fig. 5. This correction is, however, not very large, and will be neglected hereafter.

α-Phase

Structure of α-Phase. The donor arrangement of α-phase. is depicted in Fig. 7, and the geometry parameters of θ-$(ET)_2CsCo(SCN)_4$, α-$(ET)_2KHg(SCN)_4$, and α-$(ET)_2I_3$ are compared in Table 3.[5,23,24] The α-phase is generated when the periodicity of the θ-phase along the pseudo-stacking (c axis) is doubled, but no dislocation is introduced. Hence α-phase is designated as θ_{20}-structure by following the notation of Ref. 1, where 2 represents the number of molecules along the pseudo-stack and 0 stands for the number of dislocations

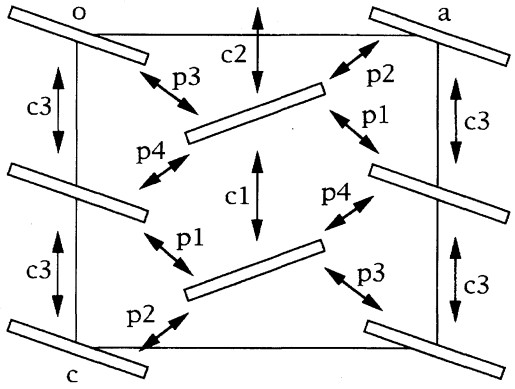

Fig. 7. Structure of the donor sheet in α-$(ET)_2KHg(SCN)_4$, viewed along the molecular long axis.

Table 3. Overlap Integrals ($\times 10^{-3}$) and Geometry Parameters in θ-$(ET)_2CsCo(SCN)_4$, α-$(ET)_2KHg(SCN)_4$, and α-$(ET)_2I_3$[4,23,24]

Interaction	Overlap $\times 10^{-3}$	$X(D)$/Å	Y/Å ($a/2$/Å)[a]	Z/Å ($c/2$/Å)[a]	ϕ/°	θ/°
θ-$(ET)_2CsCo(SCN)_4$						
c	0.5	0.0	3.0	3.8	52	180
p	−10.6	1.6	4.9	2.4		104
α-$(ET)_2KHg(SCN)_4$						
$c1$	−1.9	0.1	2.9	3.8	53	180
$c2$	6.8	0.0	3.5	3.8	48	180
$c3$	−1.2	0.0	3.0	3.8	49	174
$p1$	−10.0	1.8	4.8	2.2		98
$p2$	−9.7	1.7	4.9	2.5		106
$p3$	13.3	1.7	4.5	2.7		106
$p4$	13.2	1.7	4.6	2.5		98
α-$(ET)_2I_3$						
$c1(a1)$	3.0	0.0	1.9	4.1	65	180
$c2(a2)$	−4.9	0.0	3.5	3.8	48	180
$c3(a3)$	1.28	0.1	2.9	3.8	52	180
$p1(b1)$	−12.3	1.7	4.5	2.7		106
$p2(b2)$	−14.2	1.7	4.6	2.5		98
$p3(b3)$	6.2	1.8	4.8	2.2		98
$p4(b4)$	2.3	1.7	4.9	2.5		106

For the definition of the interactions, see Fig. 1(b) and Fig. 7. a) In these columns Y and Z defined in Fig. 1 of Ref. 1 are listed for $c1$—$c3$, and $a/2$ and $c/2$ defined in Fig. 1(a) are listed for $p1$—$p4$.

within this repeating unit. Owing to the lattice doubling, the c and p interactions of the θ-phase yield three ($c1-c3$) and four ($p1-p2$) different kinds of interactions in the α-phase, respectively (Fig. 7).

Table 3 demonstrates that, in α-$(ET)_2KHg(SCN)_4$, the distortion due to the lattice doubling is not very large. The ϕ values in each crystallographically unique stack are 53° and 48—49°, which are not largely different. The D values are nearly zero for $c1$, $c2$, and $c3$, indicating the absence of dislocation. On account of this lattice doubling, the Fermi surface of α-$(ET)_2KHg(SCN)_4$ is divided to open and closed parts (Fig. 10(d) in Ref. 1). This effect has been discussed in detail in Refs. 23 and 25.

On the contrary the lattice of *α-$(ET)_2I_3$ is significantly distorted.* The values of ϕ in the different stacks are 65° and 48—52°, respectively; this large difference means that the inclinations of each stack are significantly different. As a consequence the Fermi surface is considerably distorted in comparison with that for α-$(ET)_2KHg(SCN)_4$;[26] it separates to electron and hole pockets, and shows semimetal-like character. The band structure and the spin state have been investigated in detail as a function of the distortion when the Coulomb interaction is taken into account.[27]

Universal Phase Diagram. Lattice constants of so far reported α-phases are listed in Table 4. The notations of the crystal axes are transformed following Fig. 7. Here the entries are again aligned in the increasing order of $c/2a$; $c/2a$ is taken instead of c/a in order to facilitate the direct comparison with the θ-phase. When $c/2a$ is smaller than 0.39, the system is an insulator. Between 0.39 and 0.49 the system undergoes a M-I transition as exemplified by α-$(ET)_2I_3$. Above 0.49 the system is metal down to low temperatures. Therefore *the phase diagram of the θ-phase applies to the α-phase by shifting the axis ratio about $\Delta(c/2a) = -0.05$* (Table 2). The low-temperature insulating state of α-$(ET)_2I_3$ has been reported to be a spin singlet state.[38]

Several BETS salts with the α-phase structure have been reported (Table 4). Because M-I transitions take place in some BETS salts around $c/2a = 0.426$, the critical value of $c/2a$ is expected to be about 0.44, namely shifted by $\Delta(c/2a) = -0.06$ from the θ-phase (Table 2).

Multiple θ-Phases. Since α-phase is regarded as a multiple θ-phase, we can imagine multiple θ-phases with longer periodicities. Examples of such multiple θ-phases are listed in Table 5. The θ_{42+40}-phase has two kinds of chains which have θ_{42}-structure and θ_{40}-structure respectively. These two kinds of chains are aligned alternately in the transverse direction. This structure frequently appears when a polyanion is used as a counter anion. Because there is charge separation, many of these salts are insulators. The c/a values of these salts are small (0.364—0.373), and are located within the insulating region.

α''-Phases. In the α''-phase two types of inclination appear like ++−−++−−++−−⋯ (+ and − represent downward and upward slopes respectively) (Fig. 8(a)). The α''-phases have been reported in some ET and BO salts (Table 6).

It is characteristic of this phase that the lattice in the con-

Table 4. Lattice Parameters of α- (= θ_{20}-) Phase ET and BETS Salts

Compounds	a/Å	b/Å	c/Å	β/°	$c/2a$	T_{MI}	Ref.
α-$(ET)_2IClBr$	12.035	16.361	8.879	70.94	0.369	>300 K	28
α-$(ET)_2IBr_2$	12.031	16.402	8.905	70.86	0.370	>300 K	29
α-$(ET)_2Cu(NCS)_2$	10.854	17.471	9.052	90.37	0.417	200 K	30
α-$(ET)_2I_2Br$	10.818	17.370	9.142	90.81	0.423	265 K	31
α-$(ET)_2I_3$	10.804	17.422	9.183	90.85	0.425	135 K	24
$(ET)_2KHg(SCN)_4$	10.082	20.565	9.933	90.91	0.493	Metal	23
$(ET)_2NH_4Hg(SCN)_4$	10.091	20.595	9.963	90.53	0.494	Metal	23
$(ET)_2TlHg(SCN)_4$	10.051	20.549	9.934	90.48	0.494	Metal	32
$(ET)_2RbHg(SCN)_4$	10.050	20.566	9.965	90.57	0.496	Metal	33
$(ET)_2KHg(SeCN)_4$	10.048	20.722	9.976	90.43	0.496	Metal	34
$(ET)_2TlHg(SeCN)_4$	10.105	20.793	10.043	90.53	0.497	Metal	34
$(BETS)_2AuI_2$	10.808	17.713	9.197	90.65	0.426	45 K	19
$(BETS)_2IBr_2$	10.820	17.758	9.209	90.64	0.426	45 K	19
$(BETS)_2I_3$	10.816	17.777	9.209	90.69	0.426	45 K	19
$(BETS)_2AuBr_2$	10.76	17.16	9.25	90.7	0.430	37 K	19
$(BETS)_2NH_4Hg(SCN)_4$	10.125	20.940	9.981	90.37	0.493	Metal	35
$(BETS)_2KHg(SCN)_4$	10.069	20.925	9.968	90.28	0.495	Metal	35
$(BETS)_2HgBr_4(PhCl)_x$[a)]	9.742	75.68	9.742	90.0	0.500	Metal	36
$(BETS)_2Cu_2Cl_6$	20.043/2	34.897	9.543	90.0	0.476	Metal	37

a) This compound has a tetragonal lattice in which the donor arrangement in the conducting sheet is practically α-type.

Table 5. Lattice Parameters of Multiple θ-Phase ET Salts

Compounds	a/Å	b/Å	c/Å	c/a	T_{MI}	Ref.
θ_{31}-$(ET)_3CuBr_4$	10.123	16.937	14.078(/3)	0.467	>300K	39
θ_5+β''_5-$(ET)_5[VW_5O_{19}](H_2O)_6$	11.598	19.77	41.34(/10)	0.356	250K	40
θ_{42+40}-$(ET)_8[PMo_{12}O_{40}]PhCNH_2O$	11.375[a)]	43.260	16.575(/4)	0.364	>300K	41
θ_{42+40}-$(ET)_8[SiW_{12}O_{40}]$	11.305[a)]	43.259	16.652(/4)	0.368	>300K	42
θ_{42+40}-$(ET)_8[CoW_{12}O_{40}](H_2O)_{5.5}$	11.277[a)]	43.117	16.613(/4)	0.368	170K	43
θ_{42+40}-$(ET)_4Pt(CN)_4$	11.149	33.459	16.504(/4)	0.370	>300K	44
θ_{42+40}-$(ET)_4Ni(CN)_4$	11.123	33.313	16.506(/4)	0.371	>300K	44
θ_{42+40}-$(ET)_8[PMnW_{11}O_{39}](H_2O)_2$	11.199[a)]	43.384	16.700(/4)	0.373	>300K	45

a) The lattice has been transformed so as to correspond with the ordinary θ-phase.

ducting plane is particularly elongated. The α''-phase has a large lattice constant in the transverse direction (a axis), but a short lattice constant (about 5 Å along the pseudo-stacking (c axis) axis. Since the reciprocal lattice is inversely proportional to the real lattice, the first Brillouin zone is elongated along the pseudo-stacking direction. As a result, although the interactions of these phases are fairly isotropic in the conducting plane, the Fermi surface is open, showing one-dimensionality along the pseudo-stacking axis (Fig. 8(b)).[4,47,49]

T_{MI} of α''-phases decreases with an increase of the axis ratio, $2c/a$ (Table 6), except for $(ET)_2Cu_5I_6$, where probably the anion disorder plays an important role. Hence *the universal phase diagram applies to the α''-phase as well.* By comparing the transition temperatures with those of the ET-based θ-phases, the axis ratio is relatively shifted by about $\Delta c/a = 0.05$, so that the expected critical axis ratio is $c/a = 0.55$.

The critical values of c/a which give $T_{MI} = 0$ K, and shifts of c/a with respect to the ET-based θ-phases are summarized in Table 2. *In BETS salts the critical values shift to the negative direction, and the metal phase becomes more stable.* This is associated with the reduction of U and the enhancement of W owing to the incorporation of the more polarizable selenium atoms.

The α''-phase is a hybrid of β''-phase and θ-phase; the two chains with ++ configuration have β''-like arrangements ($p2$ and $p3$ in Fig. 8(a), and the transfers between the bundles of these two chains have θ-like arrangements ($p1$). The bundles of the two parallel chains are connected by only one kind of interaction, $p1$ along the a axis. If this $p1$ interaction becomes zero, each bundle is isolated. In this case, the band structure becomes highly one-dimensional even if the other transverse interactions $p2$ and $p3$ are large. Since the θ-like interaction $p1$ changes most sensitively as a function of the axis ratio,[46] the axis ratio regulates the degree of warping in the open Fermi surface, giving rise to the suppression of the M-I transition. Consequently, though the mechanism may be different from the case of the ordinary θ-phases (bandwidth control vs. warping control), the axis ratio controls the M-I

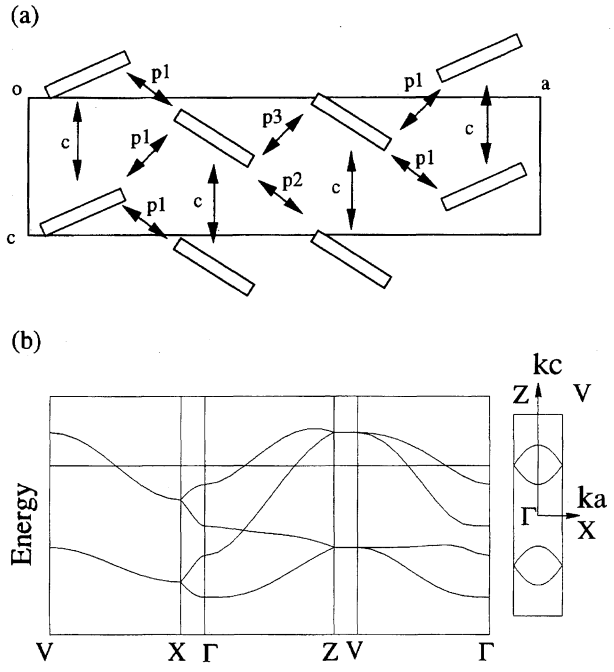

Fig. 8. (a) Structure of the donor sheet in α''-$(ET)_2Cu_5I_6$, viewed along the molecular long axis. The lattice is transformed to correspond to the ordinary θ-phases. (b) Energy band structure and Fermi surface of α''-$(ET)_2Cu_5I_6$; $b = 5.3$, $p1 = -7.5$, $p2 = -7.7$, $p3 = 16.4\times10^{-3}$.[47]

transition temperature, and the same universal phase diagram is applicable. Magnetic susceptibility of α''-phases switches from the Bonner–Fisher-like behavior to the singlet–triplet behavior in the insulating region.[46,48]

Another well-known example of α''-type stacking pattern is $[Ni(dmit)_2]$ sheet of $(TTF)[Ni(dmit)_2]_2$; this complex is the first molecular superconductor based on a metal complex (dmit: 1,3-dithiol-2-thione-4,5-dithiolate).[54]

In order to distinguish α''-structure from the ordinary θ-phase, we shall designate it as θ^{22}-phase, where the superscripts 2 represent the numbers of + and − patterns within the transverse repeating unit. According to this notation the ordinary θ-phase is denoted as θ^{11}. Theoretically long periodicities like $++-++-\cdots$ (θ^{21}-phase), $+++-+++-\cdots$ (θ^{31}-phase), etc are possible. Among these possibilities of multiple θ-phases, only one example has been known: θ^{21}-$(ET)_3Ag_{6.4}I_8$.[53]

$\varkappa$-Phase

Structue of $\varkappa$-Phase. The donor arrangement of $\varkappa$-phase is depicted in Fig. 9(a). A conducting sheet of $\varkappa$-phase is composed of dimers, which are located on both corners and centers of a rectangular lattice. The dimers on the corners are oriented in a different direction from that on the centers. The angle between these two kinds of dimers are very close to 90°. The intradimer interaction is conventionally called $b1$. There are three kinds of interdimer interactions: $b2$, p and q.

The geometry parameters of $\varkappa$-$(ET)_2Cu[N(CN)_2]Cl$, $\varkappa$-$(ET)_2Cu[N(CN)_2]Br$, $\varkappa$-$(ET)_2Cu(NCS)_2$, and $(ET)_4Hg_{3-x}Cl_8$ are listed in Table 7.[55] The geometry parameters of the $b1$ interaction are $\phi = 90°$ and $D = 1.6$ Å. This is the ordinary ring-over-bond (RB) mode, and these two molecules make a dimer.[56] Because the $\varkappa$-phase is made up of the RB mode, the molecules are significantly inclined with respect to the conducting sheet; actually the molecular long axis is inclined by $\delta = 34°$ from the direction perpen-

Table 6. Lattice Parameters of α'' ($= \theta^{22}$)-Phase ET and BO Salts

Compounds	a/Å	b/Å	c/Å	$2c/a$	θ/°	T_{MI}/K	Ref.
α''-($= \theta^{22}$-) Phase							
$(ET)_2KCu(SCN)_4$	23.086(/2)	41.112	4.257	0.369	128	Insulator	46
$(ET)_2Cu_5I_6$	22.41(/2)	21.29	4.326	0.386	125	Metal	47
$(ET)_2Au(CN)_2$	22.02(/2)	36.28	4.286	0.389	127	Insulator	48
$(ET)_2Ag(CN)_2$	22.16(/2)	36.44	4.256	0.384	125	Insulator	48
$(ET)_2CsHg(SCN)_4$	22.097(/2)	41.566	4.459	0.404	119	210 K	49
$(ET)_2K_{1.4}Co(SCN)_4$	19.18(/2)	44.639	4.93	0.514	99	130 K	5
$(BO)_5(HCP)(PhCN)_{0.2}$[a]	20.462(/2)	17.075	4.085	0.399		>300 K	50
$(BO)_6(HCDAH)$[b]	20.243(/2)	16.820	4.086	0.404		200 K	51
$(BO)_4Pt(CN)_4H_2O$	16.045(/2)	32.814	10.281(/2)	0.641		Metal	52
θ^{21}-Phase							
$(ET)_3Ag_{6.4}I_8$	16.873(/1.5)	21.115	4.4357	0.3943		60 K	53

a) HCP^{2-}: tris(dicyanomethylene)cyclopropanediide. b) $HCDAH^{2-}$: hexacyanodiazahexadiene.

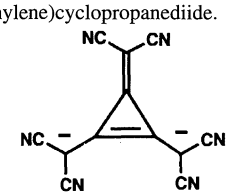

HCP^{2-}

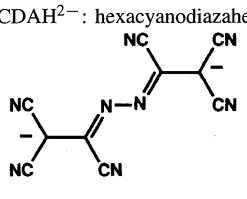

$HCDAH^{2-}$

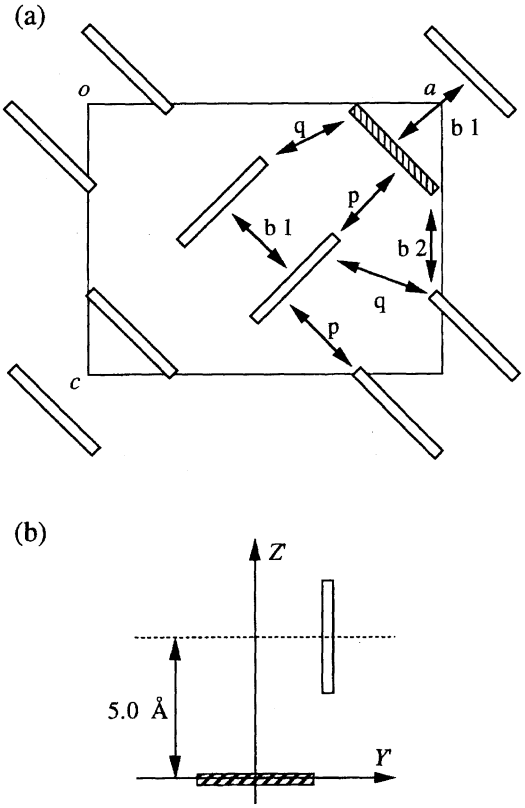

Fig. 9. (a) Structure of the donor sheet in $\varkappa$-$(ET)_2Cu[N(CN)_2]Br$, viewed along the molecular long axis. (b) Definition of "molecular coordinates" in the $\varkappa$-phase.

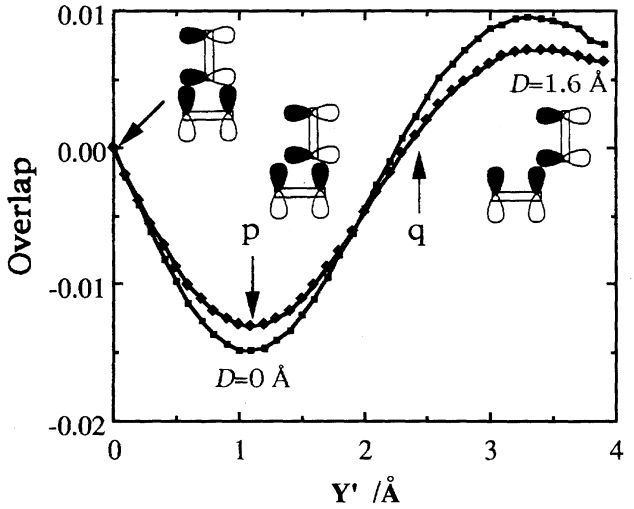

Fig. 10. Overlap integral between HOMO's of ET as a function of Y' (Fig. 9(b)).

dicular to the conducting sheet.[1] This δ is almost the same as that of the β-phase.

Owing to this inclination, the lattice in the conducting plane is not a square, but is elongated along the a axis. The dimers are connected by $b2$ along the c axis, but not connected by a parallel interaction along the a axis. In the $b2$ interaction, the molecules are again parallel to each other (Fig. 9(a)), and because ϕ is 20° (Table 7) the overlap is

Table 7. Overlap Integrals ($\times 10^{-3}$) and Geometry Parameters in $\varkappa$-$(ET)_2Cu[N(CN)_2]Cl$, $\varkappa$-$(ET)_2Cu[N(CN)_2]Br$, and $\varkappa$-$(ET)_2Cu(NCS)_2$ and $(ET)_4Hg_{3-x}Cl_8$[55,78]

Interaction	Overlap $\times 10^{-3}$	$X(D)$/Å	Y/Å (Y'/Å)[a]	Z/Å (Z'/Å)[a]	ϕ/°	θ/°
$\varkappa$-$(ET)_2Cu[N(CN)_2]Cl$ (127 K)						
$b1$	27.3	1.56	0.29	3.56	85.3	
$b2$	10.4	1.75	5.82	2.32	21.7	
p	10.5	1.98	1.07	5.07		92.2
q	3.9	3.70	2.42	4.95		92.4
$\varkappa$-$(ET)_2Cu[N(CN)_2]Br$ (127 K)						
$b1$	26.5	1.59	0.29	3.56	85.4	
$b2$	9.8	1.76	5.84	2.31	21.6	
p	10.9	2.01	1.10	5.04		92.4
q	−3.8	3.66	2.45	4.97		92.2
$\varkappa$-$(ET)_2Cu(NCS)_2$ (104 K)						
$b1$	27.2	1.67	0.15	3.53	87.6	
$b2$	11.1	1.80	5.88	2.22	21.9	
p	11.9	1.69	1.21	4.94		96.2
p'	10.5	1.88	0.97	5.04		91.0
q	−1.8	3.42	2.25	5.04		93.6
q'	−3.1	3.63	2.53	5.00		93.6
$(ET)_4Hg_{3-x}Cl_8$ (298 K)						
$b1$	24.5	1.56	0.15	3.59	87.5	
$b2$	10.5	1.22	5.68	2.93	27.3	
p	6.3	1.37	2.92	4.75		96.3
q	−3.2	3.05	1.13	5.12		96.3

a) For the definition of the interactions, see Fig. 9(a). In these columns Y and Z defined in Fig. 1 of Ref. 1 are listed for $b1$ and $b2$, and Y' and Z' defined in Fig. 9(b) are listed for p and q.

fairly large. The D value is 1.6 Å; this corresponds to half of the 1,3-dithiole ring and is the same as the ordinary transverse interactions, such as the transverse "a" interaction in the β_{21}-$(ET)_2I_3$ phase (Table 1 in Ref. 1).

The other two interactions are non-parallel. Since θ is 92° both for p and for q (Table 7), the dimers are placed almost perpendicular to each other. As shown in Figs. 3 and 4, the overlap attains a maximum around $\theta = 90°$. The oblique interactions, p and q, in $\varkappa$-phases are close to this maximum.

The geometries of p and q are obviously different. In order to investigate this difference, we shall define the coordinates of two perpendicular ET molecules as shown in Fig. 9(b). We shall place the hatched molecule on the origin, and investigate the geometry of the non-hatched molecule viewed from the hatched molecule. The Z' axis is taken perpendicular to the molecular plane of the hatched molecule, and the Y' axis is taken along the molecular short axis of this molecule. The values of Y' and Z' in actual crystals are listed in Table 7. The value of Z' is about 5.0 Å both for p and for q, then in Fig. 9(b), the non-hatched molecule is located at the same height with respect to the hatched molecule. On the contrary, the value of Y' is different.

To investigate the differences of p and q, we have calculated the overlap of the HOMO of two perpendicular ET molecules by changing Y' while keeping $Z' = 5.0$ Å (Fig. 10).

Because the HOMO has π-character, at $Y' = 0$ Å the overlap is exactly zero owing to the requirement of the symmetry. The overlap makes an extremum around $Y' = 1.1$ Å, crosses zero near $Y' = 2.2$ Å, and makes another extremum around $Y' = 3.3$ Å. *The p interaction ($Y' = 1.1$ Å) corresponds to the first extremum, but the q interaction ($Y' = 2.4$ Å) is close to zero.* Actually the calculated overlap q is very small (Table 7).

In the model calculation of the θ-phase shown in Fig. 3, if the geometry is represented by the coordinates of Fig. 9(b), the geometry at $\theta = 90°$ is $Y' = 0.8$ Å and $Z' = 5.1$ Å. This geometry corresponds to the first peak in Fig. 10, and is basically the same as the p interaction of the $\varkappa$-phase. On the other hand, in the so-called τ-phase,[57] two perpendicular donors interact with the geometry, $Y' = 3.7$ Å; this value is close to the second extremum in Fig. 10.

Energy Band Structure. The energy band structure and Fermi surface of $\varkappa$-$(ET)_2Cu(NCS)_2$ are depicted in Fig. 11(a).[58] Because q is small, it can be approximately regarded as zero. The interactions $b2$ and p are almost the same, so we can put these as $b2 = p = 11\times10^{-3}$. The resulting band structure is shown in Fig. 11(b), which is not much different from Fig. 11(a) except for the energy gap on the zone boundary. *In the real space this approximation corresponds to triangular lattice shown in Fig. 12(a), where a dimer is located on each lattice point.*[59,60]

Similarly in the θ-phase (Fig. 1), when c and p are assumed to be equal, the donors make again a triangular lattice, as shown in Fig. 12(b). In the actual θ-phase, c is not close to p but is negligibly small. Therefore in Fig. 12(b) the c interactions are designated by dashed lines. However, the band structure and the Fermi surface (Fig. 13) do not change much even if we put c as zero (Fig. 13(b)).

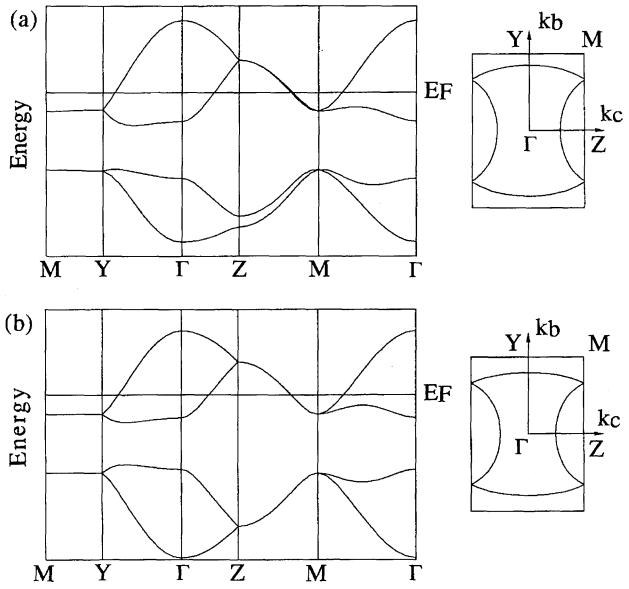

Fig. 11. Band structure and Fermi surface of the $\varkappa$-phase. (a) $\varkappa$-$(ET)_2Cu(NCS)_2$ with $b1 = 25.7$, $b2 = 10.5$, $p = 11.4$, $p' = 10.0$, $q = -1.7$, and $q' = -2.9\times10^{-3}$. (b) A simplified band with $b1 = 25.7$, $b2 = p = p' = q = q' = 11$, and $q = q' = 0\times10^{-3}$.

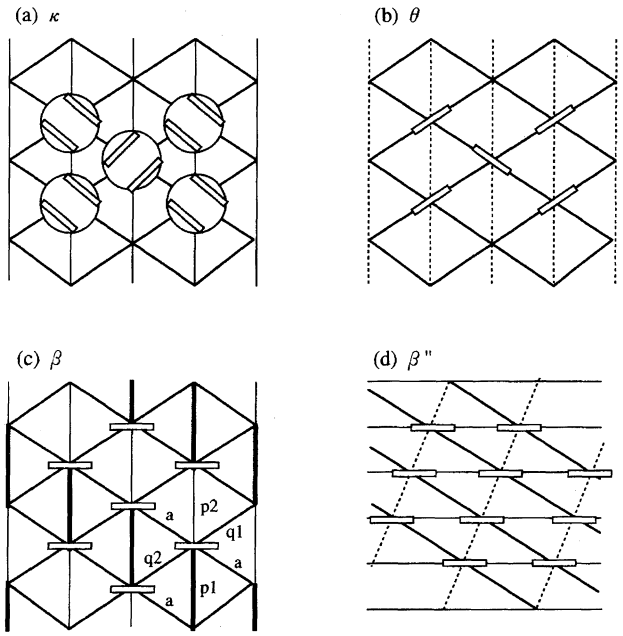

Fig. 12. Simplified intermolecular interactions in (a) $\varkappa$-, (b) θ-, (c) β-, and (d) β''-phases.

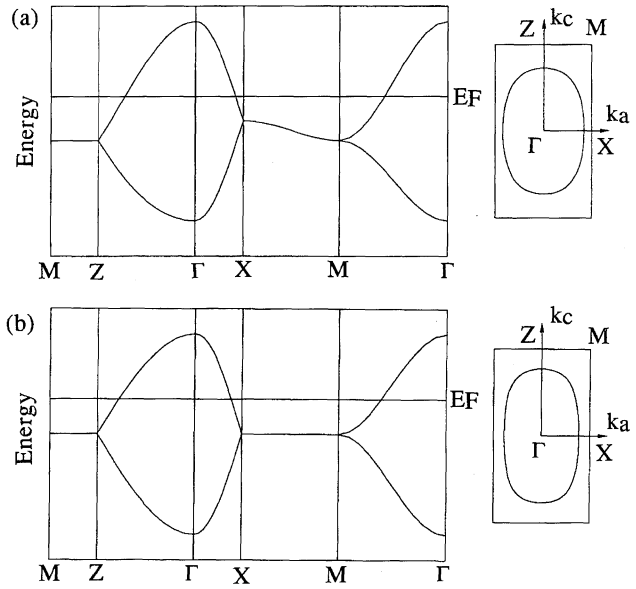

Fig. 13. Band structure and Fermi surface of a θ-phase, (a) with $c = 2$ and $q = 10\times10^{-3}$, and (b) $c = 0$ and $q = 10\times10^{-3}$.

In the θ-phase, one ET molecule, instead of one dimer, is placed on the triangular lattice. Hence we can schematically relate the $\varkappa$-phase and the θ-phase as shown in Fig. 14. If we put a dimer at the position of a molecule in the θ-phase, and slightly change the inclination, we can obtain the $\varkappa$-phase. Although this operation is entirely artificial, we can understand that in both phases the network of the interaction is made up of the oblique p interactions. In the θ-phase, the dihedral angle θ is no less than 100°; then the overlap p does not come to the maximum in Fig. 3. Yet in the $\varkappa$-phase, $\theta = 90°$ is very close to the maximum of the overlap.

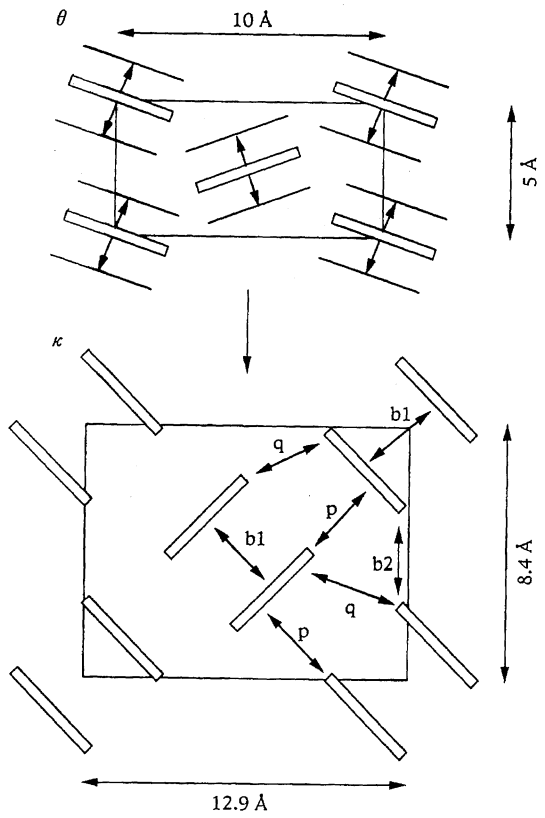

Fig. 14. Schematic relation of θ- and κ-phases.

When we go back to the reciprocal space again, on account of the dimer structure, the band structure of the κ-phase (Fig. 11) is, as a first approximation, constructed of the upper half and the lower half; these two groups of energy bands stem from the antibonding and bonding energy levels of the dimer, respectively. It has been pointed out that, in the large t_{b1} limit, the upper and lower energy bands are respectively approximated by similar formulas to Eq. 3, where t_c and t_p are replaced by $t_{b2}/2$ and $|t_p \pm t_q|/2$.[59] Since the network of the dimers is geometrically the same as the θ-phase, *the structure of the upper band is approximately the same as the band structure of the θ-phase* (compare Fig. 11 and Fig. 13).

The band filling is, however, different. Although both θ- and κ-phases have 2 : 1 composition, *in the θ-phase the entire band is quarter-filled*, and the cross section of the Fermi surface is equal to half of the first Brillouin zone. On the contrary, *in the κ-phase the upper band is effectively half-filled*, and the cross section of the Fermi surface is equal to the first Brillouin zone. If we obtain a θ-phase with 1 : 1 composition, this will have the same band structure as the κ-phase, and the Coulomb interaction will play an important role as well.[61]

Universal Phase Diagram. Taking the role of the dimerization into account, Kanoda has proposed a universal phase diagram of the κ-phase (Fig. 15).[10] In a quarter-filled band with strong dimerization, *the degree of dimerization (namely the transfer integral b1) plays the role of effective Coulomb interaction U.*[10] Therefore, when the dimerization $b1$ ($= U$) is large, the κ-phase is expected to be a paramagnetic insulator (left end in Fig. 15), which undergoes a transition to an antiferromagnetic state at low temperatures. When pressure is applied, there appears a high-temperature metal phase (center of Fig. 15), which gives rise to a superconducting phase at low temperatures.

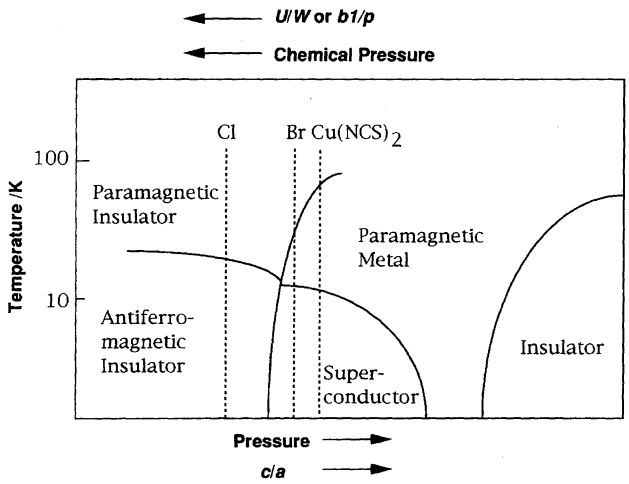

Fig. 15. Universal phase diagram of the κ-phase.

The boundary between the paramagnetic insulator and metal phases shifts to the right at high temperatures, because the thermal contraction of the lattice works as an effective pressure. So, in the intermediate region, upon cooling, the system goes from the insulator phase to the metal phase. This is the reason why in some κ-phases such as κ-$(ET)_2Cu(NCS)_2$, upon cooling, the resistivity once increases, and below 100 K it becomes metal-like again. It is worth noting that this universal phase diagram of the κ-phase resembles that of well-known V_2O_3.[62]

Chemical Pressure. When we compare the properties of κ-$(ET)_2Cu[N(CN)_2]Cl$ and κ-$(ET)_2Cu[N(CN)_2]Br$, the Cl salt is more insulating, and is obviously located at the left of the Br salt in Fig. 15. Therefore, in this phase diagram, the chemical pressure works in the opposite direction to the physical hydrostatic pressure. Not only the substitution of Br by Cl, but also the deuteration of the ET molecule leads to a slight contraction of the lattice volume, giving rise to the same effect.

In order to resolve this problem, we shall compare the overlap integrals and the lattice constants of κ-$(ET)_2Cu[N(CN)_2]Cl$, κ-$(ET)_2Cu[N(CN)_2]Br$, and κ-$(ET)_2Cu(NCS)_2$ (Table 8). When we go from the Cl salt to the Br salt, $b1$ and $b2$ decrease. Since the lattice volume increases, this is a normal chemical pressure effect. However, p increases; this is associated with the decrease of Z' in Table 7. Because Z' is directly related to the distance between the molecules, Z' changes the overlap more effectively than the other parameters.

As in the case of the θ-phase (Eq. 3), the bandwidth of the (upper half) energy band is approximated by $W = 4|t_p - t_q| \cong 4t_p$.[59] Then the ratio of $b1$ to p is regarded as an approximate measure of U/W. From the Cl salt to the Br salt $b1/p$ and accordingly U/W decreases, and the correlation becomes weak in the Br salt, resulting in the "inverse" chemical

Table 8. Overlap Integrals ($\times 10^{-3}$) and Lattice Constants of $\varkappa$-$(ET)_2CuX$[55]

X =	$N(CN)_2Cl$ 127 K		$N(CN)_2Br$ 127 K		$(NCS)_2$ 104 K
$b1$	27.3	>	26.5	<	27.2
$b2$	10.4	>	9.8	<	11.1
p	10.5	<	10.9	<	11.9, 10.5
q	−3.9		−3.8		−1.8, −3.2
$b1/p$	2.59	>	2.42		2.43
a/Å	12.909	>	12.878	>	12.855
b/Å	29.658	<	29.681	<	32.718 (/2)
c/Å	8.418	<	8.484	>	8.418
V/Å^3	3223	<	3243	<	3300 (/2)
c/a	0.652	<	0.659	>	0.655

pressure.

It is noteworthy that the lattice constant a decreases when we go from the Cl to the Br salts (Table 8). In other words, the Cl salt has a smaller c/a and a more elongated lattice in the conducting sheet. In these salts, the Cu–Cl (or Br) direction is oriented nearly along the c axis, so the lattice constant c shrinks in the Cl salt.[54] On the contrary, the anion network of $N(CN)_2$ is connected along the a axis, and the change of the coordination angles around Cu increases the lattice constant a in the Cl salt.[55] The change of the anion sheet is the origin of the anisotropic contraction induced by the chemical pressure.

Chemical pressure leads to reduction of the axis ratio c/a, which in turn results in a more correlated state. By contrast, physical pressure and thermal effect bring about a more normal contraction, giving rise to less correlated state.[63] As a consequence, physical pressure and chemical pressure work in the opposite directions.

Extended Universal Phase Diagram. We can extend this argument to other $\varkappa$-phase compounds. Lattice parameters of $\varkappa$-phase ET salts are listed in Table 9. Here we will take the notation of the crystal axes as in $\varkappa$-$(ET)_2Cu[N(CN)_2]Br$ at all times, though space group and lattice constants change from crystal to crystal. The entries are laid out in the increasing order of c/a. At the same time, a usually decreases and c increases. This corresponds to going from the left to the right in Fig. 15. Overlap integrals and some geometry parameters of representative $\varkappa$-salts are plotted as a function of c/a in Fig. 16. The horizontal axis of this figure corresponds to that of Fig. 15.

$(ET)_4Hg_{3-x}Cl_8$ is located at the right end of the figure. The geometry parameters of this salt are listed in Table 7. The angle between the dimers (96.3°) significantly deviates from 90°. In addition, the molecules are nearly parallel to the b axis ($\delta = 10°$). As a consequence the geometries of the p and q interactions are entirely different. Obviously this salt should be taken as an exception.

Many other salts are placed between $c/a = 0.64$ and 0.71. Because $b1/p$ makes a trough at $c/a = 0.675$, this figure is divided into Region I and Region II. *In both regions, as the axis ratio c/a increases, the degree of dimerization b1 decreases monotonously, because the interplanar spacing in the dimer increases.*

In Region I, as investigated in "Chemical Pressure", the interdimer interaction p increases slightly. Consequently $b1/p$ decreases. This region corresponds to the Kanoda diagram in Fig. 15. The left end of this region ($c/a<0.65$) is a highly correlated conductor, and gives rise to a paramagnetic insulator. Examples are $\varkappa$-$(ET)_2Cu[N(CN)_2]Cl$ and some samples of $\varkappa$-$(ET)_2Cu(CN)_3$, which show semiconducting behavior at ambient pressure.[65] In the intermediate c/a region ($0.64<c/a<0.69$) superconductivity appears. Near the trough ($c/a = 0.675$) is the least correlated region; for example $\varkappa$-$(ET)_2Cu[N(CN)_2]I$ exhibits a simple metal behavior down to low temperatures.

In Region II, $b1$ continues to decrease, but p *decreases significantly* (note the level of zero overlap in Fig. 16) *because the dihedral angle deviates from 90°*. As a result $b1/p$ increases remarkably. Thus the system becomes highly correlated again, and another insulating phase appears. Actually in $(ET)_2Hg(SCN)_{3-n}X_n$ family, T_{MI} increases with an increase of c/a (Table 9).

Although ESR results of these $(ET)_2Hg(SCN)_{3-n}X_n$ salts have been reported,[87] sometimes the spin susceptibility drops (for example $(ET)_2Hg(SCN)Cl_2$), and other times the Curie-like increase is observed (in $(ET)_2Hg(SCN)_2Br$), so it is difficult to derive a definite conclusion about the nature of the insulating state from the existing data.

Anisotropic Contraction. In Table 9, c/a is compared at room temperature. Thermal contraction is, however, anisotropic, and c/a may take significantly different values at low temperatures.

For example a axis of $\varkappa$-$(ET)_2Cu(NCS)_2$ shrinks as much as 7% between room and helium temperatures.[63] By contrast, the c axis shrinks about 0.9%. As a consequence the axis ratio increases to $c/a = 0.6561$ at helium temperatures. In $\varkappa$-$(ET)_2Cu[N(CN)_2]Br$ a and c axes shrink 0.6% and 1.0%, respectively, so that the axis ratio does not change much. Although the room-temperature axis ratio of $\varkappa$-$(ET)_2Cu(NCS)_2$ is located above $\varkappa$-$(ET)_2Cu[N(CN)_2]Cl$ in Table 9, suggesting a highly correlated insulating state, this low temperature value is close to $(ET)_2Cu(CF_3)_4(TCE)$, in agreement with the superconducting state. This anisotropic contraction may also be related to the semiconducting temperature dependence of the resistivity around room temperature in $\varkappa$-$(ET)_2Cu(NCS)_2$.

Thus we have to compare low-temperature lattice constants. Unfortunately data of low-temperature lattice constants are very limited. However, *the anisotropic thermal contraction is obviously associated with the existence of the polymeric anion chains.* Because the anion chains of $\varkappa$-$(ET)_2Cu(NCS)_2$ extend along the c axis, this compound shows large shrinkage along the a axis. Then c/a increases, and in Table 9 this compound moves downward. Conversely those with the polymeric chain extending along a move slightly upward in Table 9. The direction of the poly-

Table 9. Lattice parameters of $\varkappa$-Phase ET, BO, and BETS Salts

Compounds	a/Å	b/Å	c/Å	c/a[a]	S_{FS}/S_{BZ}[b]	T_{SC}	Ref.
$(ET)_4(Et_4N)Fe(CN)_6(H_2O)_3$	14.59	20.04	8.964	0.6144	0.913	Insulator	64
$(ET)_4(Et_4N)Co(CN)_6(H_2O)_3$	14.54	19.97	8.950	0.6155	0.192	Insulator	64
$\varkappa$-$(ET)_2Cu(CN)_3$	13.331	16.113	8.560	0.6421ac	(0.181)	3.8 K	65
$\varkappa$-$(ET)_2Cu(NCS)_2$	13.124	16.248	8.440	0.6431c	0.178	10.4 K	66
$(ET)_2Cu(CF_3)_4(TCE)$	13.169	38.031	8.539	0.6484	(0.172)	9.2 K	67
$(ET)_2Au(CF_3)_4(TCE)$	13.221	38.057	8.590	0.6497	(0.175)	10.5 K	68
$(ET)_2Ag(CF_3)_4(TCE)$	13.175	38.174	8.595	0.6523	(0.171)	11.1 K	67
$\varkappa$-$(ET)_2Cu[N(CN)_2]Cl$	12.977	29.979	8.480	0.6535a	(0.173)	12.5 K (0.3kbar)	54
$\varkappa$-$(ET)_2Cu[N(CN)_2]Br$	12.942	30.016	8.539	0.6598a	(0.170)	11.2 K	69
$\varkappa$-$(ET)_2I_3$	12.832	16.387	8.466	0.6598	(0.170)	3.6 K	70
$\varkappa$-$(ET)_2Cu(CN)[N(CN)_2]$	12.90	16.00	8.631	0.6691c	0.166	10.7 K	65
$\varkappa$-$(ET)_2Cu[N(CN)_2]I$	12.928	30.356	8.683	0.6716a	(0.165)	Metal	55
$\varkappa$-$(ET)_2Ag(CN)_2H_2O$	12.601	16.071	8.645	0.6861c	0.158	5.0 K	71
$(ET)_2Hg(SCN)Cl_2$	11.798	36.64	8.300	0.7035a	0.150	(T_{MI} = 35 K)	72
$(ET)_2Hg(SCN)_2I$	11.80	38.03	8.329	0.7058a	0.149	(T_{MI} = 50 K)	73
$(ET)_2Hg(SCN)_2Cl$	11.732	36.69	8.302	0.7076a	0.148	(T_{MI} = 50 K)	72
$(ET)_2(CF_3SO_3)$	11.623	34.171	8.239	0.7088	(0.148)	Insulator	74
$(ET)_2Hg(SCN)_2Br$	11.713	37.039	8.321	0.7104a	0.147	(T_{MI} = 100 K)	75
$(ET)_4PtCl_6PhCN$	11.975	17.35	8.665	0.7236	0.141	(T_{MI} = 250 K)	76
$(ET)_4Hg_{2.89}Br_8$	11.219	37.105	8.706	0.7760	(0.119)	4.3 K	77
$(ET)_4Hg_{3-x}Cl_8$	11.062	35.92	8.754	0.7914	(0.113)	1.8 (12 kbar)	78
$(BO)_2CF_3SO_3$	10.427	34.396	7.955	0.7629	(0.124)	(T_{MI} = 150 K)	79
$(BETS)_2Cu[N(CN)_2]Br$	12.961	31.005	8.576	0.6617a	(0.169)	Metal	80
$(BETS)_2AsF_6(TCE)_x$	12.052	38.219	8.406	0.6975	(0.153)	Metal	19
$(BETS)_2PF_6(TCE)_x$	12.005	38.022	8.387	0.6986	(0.152)	Metal	19
$(BETS)_2CF_3SO_3$	11.732	34.972	8.332	0.7102	(0.147)	(T_{MI} = 30 K)	81
$(BETS)_2TlI_4$	11.902	41.067	8.532	0.7169	(0.144)	Insulator	35
$\varkappa$-$(BETS)_2TaF_6$	11.636	35.163	8.362	0.7186	(0.143)	Metal	18
$\varkappa$-$(BETS)_2GaBr_4$	11.773	36.635	8.492	0.7213	(0.142)	Metal	82
$\varkappa$-$(BETS)_2FeBr_4$	11.754	36.530	8.482	0.7216	(0.142)	Metal	82
$\varkappa$-$(BETS)_2GaCl_4$	11.665	35.894	8.464	0.7258	(0.140)	Metal	82
$\varkappa$-$(BETS)_2FeCl_4$	11.693	35.945	8.491	0.7261	(0.140)	Metal	83
$(BETS)_4Cu_2Cl_6$	11.531	34.797	8.449	0.7327	(0.137)	(T_{MI} = 40 K)	84
$(BETS)_2SbF_6$	11.511	35.310	8.434	0.7327	(0.137)	Metal	19
$(BETS)_2InCl_4$	11.586	36.492	8.536	0.7367	(0.135)	Metal	82
$(BETS)_2TlCl_4$	11.600	36.577	8.553	0.7373	(0.135)	Metal	35
$(BETS)_xHgBr_y$	11.516	39.064	8.654	0.7515	(0.129)	Metal	36
$(BETS)_2BF_4(TCE)_x$	22.568/2	19.122	8.559	0.7585	(0.126)	Metal	85
$(BETS)_2ClO_4(TCE)_x$	22.551/2	19.253	8.568	0.7599	(0.126)	Metal	85

a) Those with "a" after the number have polymeric anion chains running along the a axis, "c" means chains along the c axis, and no sign stands for discrete anions. b) Cross section of the closed Fermi surface estimated from Eq. 8 in Appendix. Those designated in parentheses have, on account of the existence of glide planes, no energy gap on the zone boundary

meric chains is designated after c/a in Table 9. If we take this correction into account, M-I and superconducting transitions of $\varkappa$-phase salts are well accounted for by a single phase diagram.

Cross Section of Fermi Surface. In the $\varkappa$-phase compounds, the cross section of closed orbit of the Fermi surface (S_{FS}/S_{BZ}) is also related to the value of c/a. Assuming a perfectly circular Fermi surface, without carrying out the band calculation, we can estimate S_{FS}/S_{BZ} only from c/a after a few geometrical calculations (Appendix). The values of S_{FS}/S_{BZ} are listed in Table 9.

The value S_{FS}/S_{BZ} = 0.17—0.18 is the same as the result of the band calculation, and also agrees well with the experimental results of quantum oscillations.[88] From this viewpoint, we can consider that the network of the $\varkappa$-phase has a perfect two-dimensional character. As listed in Table 9, the larger c/a is, the smaller S_{FS}/S_{BZ} becomes. This tendency is, however, not obvious from the band calculation of the individual salts. Unfortunately, all salts in which quantum oscillations have been observed so far are located near S_{FS}/S_{BZ} = 0.17.[88] In the future, if quantum oscillations of $\varkappa$-phases with extreme c/a values or band filling other than the quarter filled (ρ = 0.5) are observed, it will be interesting to compare the results with the present relations.

BO and BETS Salts. As discussed in "θ-Phase", $\varkappa$-phases based on BO and BETS are expected to follow the same phase diagram as well. There has been reported only one BO-based $\varkappa$-phase, $(BO)_2CF_3SO_3$ (Table 9); this salt

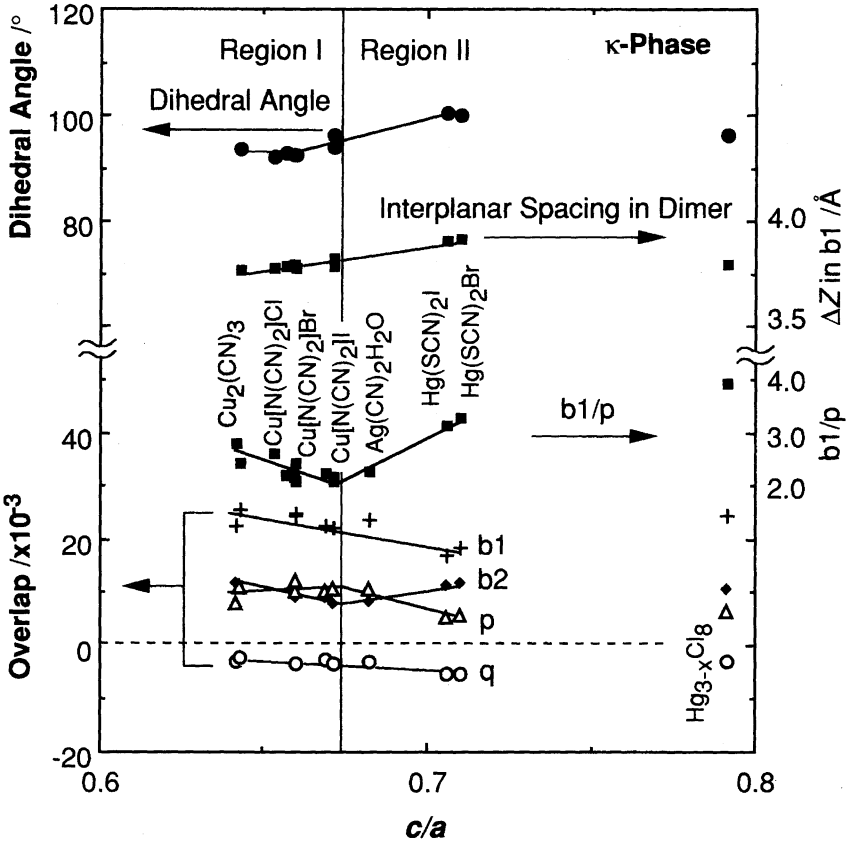

Fig. 16. Dihedral angle, interplanar distance in the dimer, ratio of overlap integrals, $b1/p$, and overlap integrals in $\varkappa$-phase ET-salts.[86]

exhibits an M-I transition at 150 K.[79] Since this salt takes comparatively large *c/a*, this salt is placed in Region II in Fig. 16, and the M-I transition is considered to be the same kind as that of the $(ET)_2Hg(SCN)_2X$ family.

There are many BETS-based $\varkappa$-salts (Table 9). The range of *c/a* values (0.69—0.76) is in general larger than that of the ET salts (most salts fall into the region of 0.64—0.71). By analogy with Fig. 16, this leads to a smaller $b1$ and a less correlated state. Furthermore, when we have compared the phase diagrams of ET and BETS in the θ-phase, we have concluded that U of BETS is comparatively small. These are the origins of the simple metal state observed in many BETS-based $\varkappa$-salts.

Comparison of θ- and $\varkappa$-Phase. The analogy of the universal phase diagrams of the $\varkappa$-phase (Fig. 15) and the θ-phase (Fig. 5) is obvious. Horizontal axes of both phase diagrams are able to be regarded as *c/a*. It is common to both phase diagrams that in small *c/a* a paramagnetic insulating state appears.

In the θ-phase, the substitution of Cs atoms of $(ET)_2CsZn(SCN)_4$ by smaller Rb atoms leads to the increase of T_{MI} from 20 to 190 K. This is associated with the decrease of *c/a*. Therefore *both θ- and $\varkappa$-phases show the same chemical pressure effect*, which reduces *c/a*, and gives rise to a correlated insulating state.

However, *physical pressure works inversely*. In the θ-phase physical pressure as well as chemical pressure causes the decrease of *c/a*, and raises T_{MI}, as demonstrated in $(ET)_2MM'(SCN)_4$ series compounds.[6,9] In the $\varkappa$-phase, pressure works so as to reduce the correlation, and stabilizes the metallic state. If thermal contraction is assumed to work in the same direction as the physical pressure, this difference explains the inclination of the M-I boundary. In $\varkappa$-phases thermal contraction as well as pressure reduces the correlation, so that the boundary between the paramagnetic insulator and the paramagnetic metal shifts to the right as temperature rises (Fig. 15). Contrarily thermal contraction enhances the correlation in θ-phases, and the boundary turns to the left in Fig. 5.

It should be also noted that the range of *c/a* which emerges in actual crystals is comparatively narrow in the $\varkappa$-phase; most salts fall within 0.64 and 0.69, and the interval is 0.05. By contrast the θ-phase takes the values between 0.35 and 0.52, with an interval of 0.17. This is the reason that θ-phases exhibit a large variety of properties, from an insulating state even at room temperature to a metallic state.

Simplified Interactions

We have shown that, when the interactions of the θ- and $\varkappa$-phases are simplified so as to have triangular interactions (Fig. 12), the resulting band structures are essentially the same as the actual ones (Figs. 11 and 13).

Similarly we may simplify the interactions of the β-phase as in Fig. 12(c), where the thick lines represent the dimers. In this case, however, if we put all the inter-dimer interactions equal ($p2 = q1 = a$), in any choice of the parameters, we

have been unable to reproduce the closed Fermi surface. A somewhat larger $q1$ seems to be essential to make the Fermi surface closed.

As another possibility, we may take the dimer as a unit. The combination of one $q2$ and two a interactions connect the dimers in one direction, just as $p2$ and $q1$ interactions connect the dimers in the other directions. The magnitudes of the $q2$ and a interactions are comparatively small, so as to make a reasonably balanced interaction of the triangular lattice. Anyway, the interactions of the β-phase are able to be regarded as those of a modified triangular lattice.

The interactions of the β''-phase (Fig. 12(d)) are again represented by a distorted triangular lattice as shown in Fig. 12(d).

Favored Structures of Each Donor

In the present work, we have investigated various salts of ET, BO, and BETS, listed in Tables 1, 4, 5, 6, and 9. Together with the tables shown in Ref. 1, these tables cover 64%, 80%, and 83% of all reported ET, BO, and BETS salts, respectively. Some salts are not included, either because sufficient information to discuss the structure has not been given, or because the anions are included in the donor sheet so that the salts do not make a conducting sheet and the classification described in the present paper is of no use. The latter types of structures are frequently observed, but are usually poor electrical conductors. However, even in these salts, the overlap integrals between the donors are able to be discussed according to the principles of the present work.

Table 10 summarizes the numbers of salts with each structure type. From this we can discuss which structure is favored by each donor. For example BO has a strong tendency to form β''-structure; 15 in 20 of salts reported take the β''-structure.

In Ref. 1, we have discussed the ring-over-bond (RB) and ring-over-atom (RA) overlap modes as the essential building blocks. The RB mode makes the usual stacks, as observed in β-phases, but the RA mode affords pseudo-stacks extending in the $\phi = 60°$ direction with respect to the molecular plane. The β''-, θ-, and α-phases are composed of the RA overlap mode. Then we shall consider the statistical probability that the RA overlap mode appears in each donor. We shall define "RA number" as RA = 0 for the salts constructed only of the RB mode, namely for β- and $\varkappa$-phases, and RA = 1 for the salts made up of the RA mode, namely for β''-, θ-, and α-phases (Table 10). Since the β'-phase has both modes, the RA number is 0.5. Then we shall average the RA numbers for all reported salts. From Table 10, the RA numbers are calculated to be 0.66, 0.95, and 0.39 for ET, BO, and BETS, respectively. These numbers represent the statistical probability that the RA mode appears.

Table 10. Numbers of ET, BO, and BETS Salts with Each Structure Type

Phase	ET	BO	BETS	RA[a)]	Inclination[b)]
β	18	0	2	0.0	0.0
β'	7	0	0	0.5	0.0
β''	37	15	0	1.0	0.0
θ	15	1	4	1.0	0.66
α	19[c)]	0	8	1.0	0.66
α''	7[d)]	3	0	1.0	0.33
$\varkappa$	21	1	17	0.0	0.66
$\delta(\beta\text{-}PF_6)$	20	0	0	—	—
α'	13	0	0	—	—

a) RA number: probability of the RA mode. b) Inclination number: probability of inclined interactions. c) Including multiple θ-phases listed in Table 4. d) Including one θ^{21}-phase listed in Table 5.

We have frequently encountered the inclined interactions where the molecular planes are not parallel. We shall then consider the statistical probability of such inclined interactions. We shall also define "inclination number". For instance, in the $\varkappa$-phase (Fig. 9(a)), $b1$ and $b2$ are parallel interactions, but p and q are inclined interactions. Since p and q appear twice when $b1$ and $b2$ appear once in a repeating unit, we shall define the inclination number as $4/6 = 0.66$. The inclination numbers of various phases are listed in Table 10. By summing up the inclination numbers for each donor, we can obtain the inclination numbers of ET, BO, and BETS as 0.31, 0.12, and 0.62, respectively.

We can obtain these numbers also for various donors other than ET, BO and BETS. In Fig. 17, several donors are plotted with respect to the RA number (horizontal) and the inclination number (vertical). Every time a new salt is found, the position of the donor in Fig. 17 should move slightly. However, this plot represents well the favored structures of each donor, particularly when a large number of salts have been reported already. Table 10 contains δ- and α'-phases, but we cannot define RA number and inclination number in these phases. So these phases must be excluded in the present discussion.

In Fig. 17, each corner represents four typical structures: β, β'', $\varkappa$, and θ. The bottom edge is sandwiched by β and β'', in which all molecular planes are parallel to each other. On the upper edge $\varkappa$ and θ are located; here the inclined interaction plays an important role. The isotropic nature in the two-dimensional conducting sheet is more perfectly attained when we go from the lower to the upper part.

The salts on the left edge are made up of the RB overlap mode, and δ angles (inclination of the molecular plane with respect to the conducting sheet) are usually large.[1)] It should be also pointed out that dimerization is inherent to the RB mode. The RA mode is predominant on the right edge. In the RA mode the molecules are slid along the molecular short axis, and further dimerization is not necessary or very weak. In general structures in the left of Fig. 17 show a stronger tendency to dimerization.

ET is placed near the center of the diagram, indicating a rich variety of structures. The RA number 0.66 means that the RA overlap mode appears more frequently (in about two-thirds of the salts) than the RB mode. BO is placed very close to the β''-corner; β''-phase is predominant except for only one $\varkappa$-salt and one θ-salt. Most BETS salts take θ- or $\varkappa$-structure; the existence of two λ-salts causes the deviation

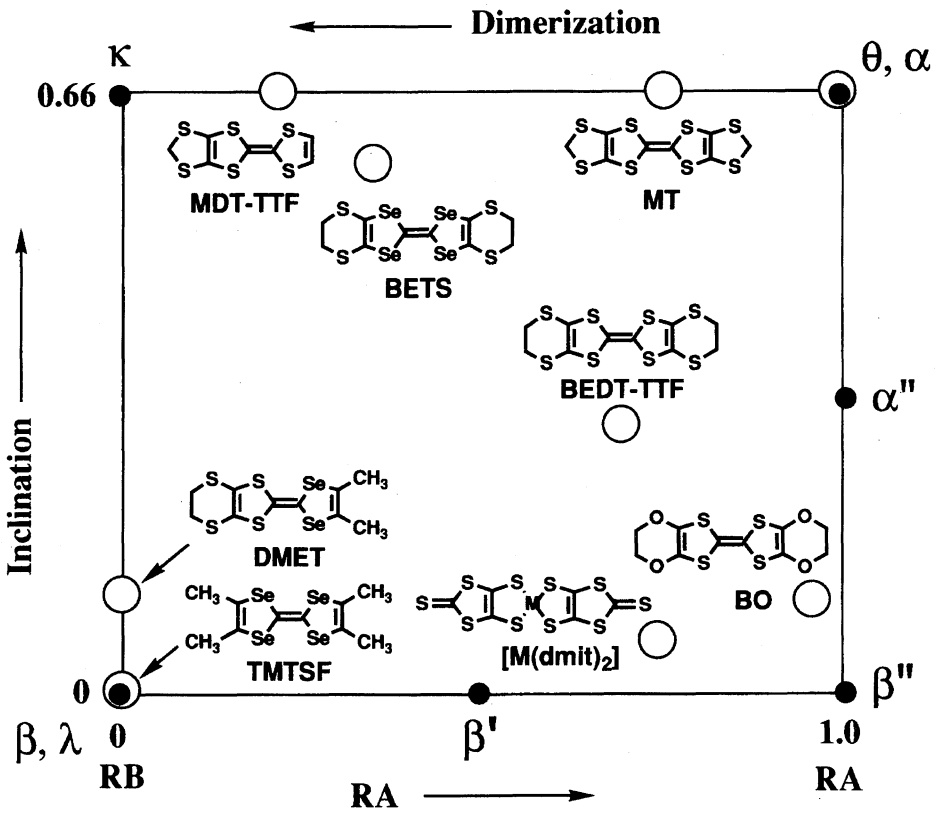

Fig. 17. RA numbers and inclination numbers in various donors.

from the upper edge.

As for MT and MDT-TTF, only θ- and $\varkappa$-salts have been known; so these donors are located on the upper edge. Because all TMTSF salts have regular stacks, both RA and inclination numbers are zero, then TMTSF is situated on the left bottom corner. The hybrid of TMTSF and BEDT-TTF, namely DMET, usually takes a TMTSF-type structure; but $(DMET)_2AuBr$ is $\varkappa$-type, so the average inclination increases slightly. Metal dmit salts frequently take β''-like structure, but some interactions are more β-like; the dmit salts sometimes realize interactions with $\phi = 70°$—$80°$.[89] There also appears θ-like stacking. As a result, the metal dmit is located a little below ET.

The position in this plot represents what kind of structure is favored by each donor. The conventional organic donors which form one-dimensional chains, like TMTSF, should be placed at the left bottom corner. BO, ET, and BETS are located far from this corner, indicating the two-dimensional nature of these salts. When we trace from BO, ET, to BETS, they are placed on the line running from the right bottom to the left top.

Such donors as BETS and MT are designed so as to have similar widths of the inner and outer rings.[90] In BETS, sulfur atoms of the inner five-membered rings of ET are replaced by selenium; this enlarges the width of the inner ring, to enhance the transverse interaction. In MT the outer six membered rings of ET are replaced by five-membered rings. It is noteworthy that these donors are located near the top of the diagram, and the inclined interactions are the major driving force to their two dimensionality.

On the contrary, BO and metal dmit salts favor β''-type structures; these molecules are located near the right bottom corner. In particular, BO shows great favor to the RA overlap mode. This "self-aggregation" of BO molecules has been attributed to the ability to form weak hydrogen bonds.[50] In BO and metal dmit salts, preference for the RA overlap mode makes their crystals two-dimensional.

In summary, from the model calculation of intermolecular overlap integrals, we have shown that the inclined interaction increases with an decrease of the dihedral angle θ. In θ-phase, this leads to a large increase (0.15 to 0.8 eV) of the bandwidth and the transition from a correlated insulator to a simple metal state (universal phase diagram).

Since c/a changes in proportion to the dihedral angle, we can use c/a instead of the dihedral angle to plot these salts. The same universal phase diagram is applicable to the related phases such as α and α'', and the corresponding phases of other donors.

Salts of $\varkappa$-phase are similarly plotted with respect to c/a. The diagram is separated into two c/a regions (Region I and II), where the decreases of the intradimer overlap integral, $b1$, and the interdimer interaction, p, work competitively, leading to two different insulating phases at both ends of the c/a plot.

In both θ- and $\varkappa$-phases, chemical pressure reduces c/a, and stabilizes the insulating state. Physical pressure in θ-phase works in the same direction as the chemical pressure, whereas in $\varkappa$-phase hydrostatic pressure enhances the interdimer interaction, and gives rise to an opposite influence.

To investigate the favored phases of each donor, RA and inclination numbers are defined. A plot with regard to these numbers illustrate the characteristics of each donor. In BETS and MT, the inclined interaction is the predominant driving force to make the electronic states of their crystals two-dimensional. By contrast the RA overlap mode is important in BO and metal dmit salts.

The applicability of the universal phase diagram is characteristic of these phases made up of the inclined interactions (θ- and $\varkappa$-phases). This makes a sharp contrast with β- and β''-phases, where the introduction of dislocation leads to various multiple phases.

The authors are grateful to Dr. T. Komatsu who permitted us to use his results of band calculation for our plot in Fig. 16.[86]

Appendix

If we assume that the Fermi surface of the $\varkappa$-Phase is a perfect circle, we can estimate the cross section of the closed orbit (shaded area in Fig. 18) only from the ratio of the lattice constants. The area of the first Brillouin zone is $S_{BZ} = \frac{4\pi^2}{ac}$. Since the area of the circle is equal to this area, the radius of the circle is given by $\overline{\Gamma Q} = \sqrt{\frac{4\pi}{ac}}$, and the angle $\angle Q\Gamma X$ is obtained as

$$\angle Q\Gamma X = \cos^{-1}\frac{\overline{OX}}{\overline{OQ}} = \cos^{-1}\sqrt{\frac{\pi}{4}\frac{c}{a}}. \tag{5}$$

The area of the triangle $Q\Gamma X$ is represented as

$$\Delta Q\Gamma X = \frac{1}{2}\frac{\pi}{a}\sqrt{\frac{4\pi}{ac} - \left(\frac{\pi}{a}\right)^2}, \tag{6}$$

and the area of fan $Q\Gamma P$ is

$$\frac{2\pi}{ac}\cos^{-1}\sqrt{\frac{\pi}{4}\frac{c}{a}}. \tag{7}$$

Equation 5 is subtracted from Eq. 6, multiplied by 4, and divided by S_{BZ} to afford:

$$\frac{S_{FS}}{S_{BZ}} = \frac{2}{\pi}\cos^{-1}\sqrt{\frac{\pi}{4}\frac{c}{a}} - \sqrt{\frac{c}{\pi a} - \frac{1}{4}\left(\frac{c}{a}\right)^2}. \tag{8}$$

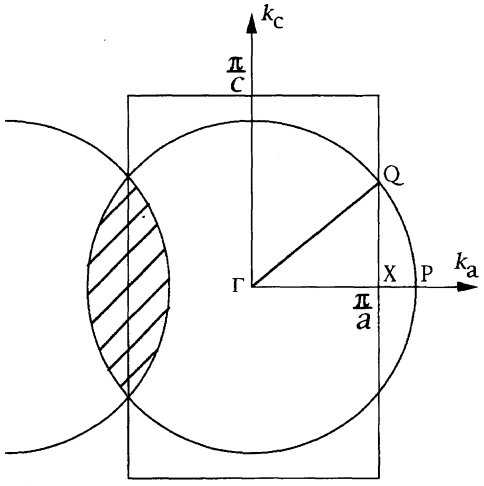

Fig. 18. Schematical representation of the Fermi surface of the $\varkappa$-phase.

If the degree of charge transfer ρ is deviated from one quarter, the Fermi surface is 4ρ times larger, and the final result becomes:

$$\frac{S_{FS}}{S_{BZ}} = \frac{2}{\pi}\cos^{-1}\sqrt{\frac{\pi}{16\rho}\frac{c}{a}} - \sqrt{\frac{4\rho}{\pi}\frac{c}{a} - \frac{1}{4}\left(\frac{c}{a}\right)^2}. \tag{9}$$

References

1) T. Mori, *Bull. Chem. Soc. Jpn.*, **71**, 2509 (1998).
2) T. Mori, A. Kobayashi, Y. Sasaki, H. Kobayashi, G. Saito, and H. Inokuchi, *Bull. Chem. Soc. Jpn.*, **57**, 627 (1984).
3) T. Mori, in preparation.
4) H. Mori, S. Tanaka, T. Mori, and Y. Maruyama, *Bull. Chem. Soc. Jpn.*, **68**, 1136 (1995).
5) H. Mori, S. Tanaka, and T. Mori, *Mol. Cryst. Liq. Cryst.*, **284**, 15 (1996).
6) T. Mori, A. Fuse, H. Mori, and S. Tanaka, *Physica C*, **264**, 22 (1996).
7) H. Mori, S. Tanaka, and T. Mori, *J. Phys. I, France*, **6**, 1987 (1996).
8) H. Mori, S. Tanaka, T. Mori, A. Kobayashi, and H. Kobayashi, *Bull. Chem. Soc. Jpn.*, **71**, 797 (1998).
9) H. Mori, S. Tanaka, and T. Mori, *Phys. Rev. B*, **57**, 12023 (1998).
10) K. Kanoda, *Hyperfine Interact.*, **104**, 235 (1997).
11) U. Geiser, H. H. Wang, P. R. Rust, L. M. Tonge, and J. M. Williams, *Mol. Cryst. Liq. Cryst.*, **181**, 117 (1990).
12) T. Komatsu, H. Sato, T. Nakamura, N. Matsukawa, H. Yamochi, G. Saito, M. Kusunoki, K. Sakaguchi, and S. Kagoshima, *Bull. Chem. Soc. Jpn.*, **68**, 2233 (1995).
13) U. Geiser, M. A. Beno, A. M. Kini, H. H. Wang, A. J. Schultz, B. D. Gates, C. S. Cariss, K. D. Carlson, and J. M. Williams, *Synth. Met.*, **27**, A235 (1988).
14) M. Kurmoo, D. R. Talham, K. L. Pritchard, P. Day, A. M. Stringer, and J. A. K. Howard, *Synth. Met.*, **27**, A177 (1988).
15) H. Kobayashi, R. Kato, A. Kobayashi, Y. Nishio, K. Kajita, and W. Sasaki, *Chem. Lett.*, **1986**, 789, 833, and 957; K. Kajita, Y. Nishio, S. Moriyama, W. Sasaki, R. Kato, H. Kobayashi, and A. Kobayashi, *Solid State Commun.*, **64**, 1279 (1987).
16) H. H. Wang, U. Geiser, S. K. Kumar, A. C. Cooper, J. A. Schlueter, A. M. Kini, A. J. Skulan, M. L. Vanzile, J. Dudek, J. M. Williams, D. G. Hinks, and W.-K. Kwok, *Mol. Cryst. Liq. Cryst.*, **284**, 437 (1996).
17) D. Schweitzer, S. Kahlich, I. Heinen, S. E. Lan, B. Nuber, H. J. Keller, K. Winzer, and H. W. Helberg, *Synth. Met.*, **56**, 2827 (1993); E. I. Zhilyaeva, S. A. Torunova, R. N. Lyubovskaya, S. V. Konovalikhin, O. A. Dyachenko, R. B. Lyubovskii, and S. I. Pesotskii, *Synth. Met.*, **83**, 7 (1996).
18) R. Kato, A. Kobayashi, A. Miyamoto, and H. Kobayashi, *Chem. Lett.*, **1991**, 1045.
19) R. Kato, H. Kobayashi, and A. Kobayashi, *Synth. Met.*, **42**, 2093 (1990).
20) S. Golhen and L. Ouahab, *Synth. Met.*, in press.
21) M. Tamura, K. Yakushi, H. Kuroda, A. Kobayashi, R. Kato, and H. Kobayashi, *J. Phys. Soc. Jpn.*, **57**, 3239 (1988); M. Tamura, H. Kuroda, S. Uji, H. Aoki, M. Tokumoto, A. G. Swanson, J. S. Brooks, C. C. Agosta, and S. T. Hannahs, *J. Phys. Soc. Jpn.*, **63**, 615 (1994).
22) J. M. Williams, H. H. Wang, T. J. Emge, U. Geiser, M. A. Beno, P. C. W. Leung, K. D. Carlson, R. J. Thorn, A. J. Schultz, and M.-H. Whangbo, *Prog. Inorg. Chem.*, **35**, 51 (1987). The authors

of this paper have confined themselves to the β and β'' phases, and the pattern of the θ-phase has been called W-mode without the distinction of L-mode and Z-mode. We can, however, easily extend this distinction to θ-phases.

23) H. Mori, S. Tanaka, M. Oshima, G. Saito, T. Mori, Y. Maruyama, and H. Inokuchi, *Bull. Chem. Soc. Jpn.*, **63**, 2183 (1990).

24) K. Bender, I. Hennig, D. Schweizer, K. Dietz, H. Endres, and H. J. Keller, *Mol. Cryst. Liq. Cryst.*, **108**, 359 (1984).

25) S. Ono, T. Mori, S. Endo, N. Toyota, T. Sasaki, Y. Watanabe, and T. Fukase, *Physica C*, **290**, 49 (1997).

26) N. Tajima, T. Mishima, M. Tamura, Y. Nishio, and K. Kajita, *Synth. Met.*, **86**, 2005 (1997).

27) H. Kino and H. Fukuyama, *J. Phys. Soc. Jpn.*, **64**, 1877 and 4523 (1996).

28) H. Kobayashi, R. Kato, A. Kobayashi, G. Saito, M. Tokumoto, H. Anzai, and T. Ishiguro, *Chem. Lett.*, **1986**, 33.

29) J. M. Williams, H. H. Wang, M. A. Beno, T. J. Emge, L. M. Sowa, P. T. Copps, F. Behroozi, L. N. Hall, K. D. Carlson, and G. W. Crabtree, *Inorg. Chem.*, **23**, 3839 (1984); E. B. Yagubskii, I. F. Shchegolev, R. P. Shibaeva, D. N. Fedutin, L. P. Rozenberg, E. M. Sogomonyan, R. M. Lobkovskaya, V. N. Laukhin, A. A. Ignat'ev, A. V. Zvarykina, and L. I. Buravov, *JETP Lett.*, **42**, 206 (1985).

30) N. Kinoshita, K. Takahashi, K. Murata, M. Tokumoto, and H. Anzai, *Solid State Commun.*, **67**, 465 (1988).

31) D. Zhu, P. Wang, M. Wan, Z. Yu, and N. Zhu, *Solid State Commun.*, **57**, 843 (1986).

32) A. I. Shchegolev, V. N. Laukhin, A. G. Khomenko, M. V. Kartsovnik, R. P. Shibaeva, L. P. Rozenberg, and A. E. Kovalev, *J. Phys. I*, **2**, 2123 (1992); L. I. Buravov, N. D. Kushch, V. N. Laukhin, A. G. Khomenko, E. B. Yagbuskii, M. V. Kartsovnik, A. E. Kovalev, L. P. Rozenberg, R. P. Shibaeva, M. A. Tanatar, V. S. Yefanov, V. V. Dyakin, and V. A. Bondarenko, *J. Phys. I*, **4**, 441 (1994).

33) H. Mori, S. Tanaka, K. Oshima, G. Saito, T. Mori, Y. Maruyama, and H. Inokuchi, *Synth. Met.*, **42**, 2013 (1991).

34) T. Sasaki, H. Ozawa, H. Mori, S. Tanaka, T. Fukase, and N. Toyota, *J. Phys. Soc. Jpn.*, **65**, 213 (1996).

35) L. K. Montgomery, B. W. Fravel, J. C. Hoffman, C. C. Agosta, and S. A. Ivanov, *Synth. Met.*, **85**, 1521 (1997).

36) T. Naito, A. Miyamoto, H. Kobayashi, R. Kato, and A. Kobayashi, *Chem. Lett.*, **1991**, 1945.

37) A. Kobayashi, A. Sato, E. Arai, H. Kobayashi, C. Faulmann, N. Kushch, and P. Cassoux, *Solid State Commun.*, **103**, 371 (1997).

38) B. Rothanemel, L. Forro, J. R. Cooper, J. S. Schilling, M. Weger, P. Bele, H. Brunner, D. Schweitzer, and H. J. Keller, *Phys. Rev. B*, **34**, 704 (1986).

39) T. Mori, F. Sakai, G. Saito, and H. Inokuchi, *Chem. Lett.*, **1997**, 927.

40) S. Triki, L. Ouahab, D. Grandjean, R. Canet, C. Garrigou-Lagrange, and P. Delhaes, *Synth. Met.*, **56**, 2028 (1993).

41) C. Bellitto, M. Bonamico, V. Fares, F. Federici, G. Righini, M. Kurmoo, and P. Day, *Chem. Mater.*, **7**, 1475 (1995).

42) A. Davidson, K. Boubekeur, A. Penicaud, P. Auban, C. Lenoir, P. Batail, and G. Herve, *J. Chem. Soc., Chem. Commun.*, **1989**, 1373.

43) J. Gomez-Garcia, L. Ouahab, C. Gimenez-Saiz, S. Triki, E. Coronado, and P. Delhaes, *Angew. Chem., Int. Ed. Engl.*, **33**, 223 (1994).

44) M. Fettouhi, L. Ouahab, D. Grandjean, L. Ducasse, J. Amiell, R. Canet, and P. Delhaes, *Chem. Mater.*, **7**, 461 (1995).

45) J. R. Galan-Mascaros, C. Gimenez-Saiz, S. Triki, J. Gomez-Garcia, E. Coronado, and L. Ouahab, *Angew. Chem., Int. Ed. Engl.*, **34**, 1460 (1995).

46) H. Mori, T. Okano, N. Sakurai, S. Tanaka, K. Kajita, and H. Moriyama, *Chem. Lett.*, **1998**, 505.

47) R. P. Shivaeva and R. M. Lobkovskaya, *Sov. Phys. Crystallogr.*, **33**, 241 (1988); T. Mori and H. Inokuchi, in "The Physics and Chemistry of Organic Superconductors," ed by G. Saito and S. Kagoshima, Springer, Berlin (1990), p. 204.

48) M. Kurmoo, P. Day, T. Mitani, H. Kitagawa, H. Shimoda, D. Yoshida, P. Guionneau, Y. Barrans, D. Chasseau, and L. Ducasse, *Bull. Chem. Soc. Jpn.*, **69**, 1233 (1996).

49) H. Mori, S. Tanaka, T. Mori, Y. Maruyama, H. Inokuchi, and G. Saito, *Solid State Commun.*, **78**, 49 (1991).

50) S. Horiuchi, H. Yamochi, G. Saito, K. Sakaguchi, and M. Kusunoki, *J. Am. Chem. Soc.*, **118**, 8604 (1996)

51) H. Yamochi, K. Tsutsumi, T. Kawasaki, and G. Saito, *Mat. Res. Soc. Sympo. Proc.*, **488**, 641 (1998).

52) E. I. Zhilyaeva, R. N. Lyubovskaya, S. A. Torunova, S. V. Konovalikhin, O. A. Dyachenko, and P. B. Lyubovskii, *Synth. Met.*, **80**, 91 (1996).

53) U. Geiser, H. H. Wang, K. M. Donega, B. A. Anderson, J. M. Williams, and J. F. Kwak, *Inorg. Chem.*, **25**, 401 (1986); U. Geiser, H. H. Wang, J. M. Williams, E. L. Venturini, J. F. Kwak, and M.-H. Whangbo, *Synth. Met.*, **19**, 599 (1987).

54) M. Bousseau, L. Valade, M.-F. Bruniquel, P. Cassoux, M. Garbauskas, L. Interrante, and J. Kasper, *Nouv. J. Chim.*, **4**, 3 (1984).

55) U. Geiser, A. J. Schultz, H. H. Wang, D. M. Watkins, D. L. Stupka, J. M. Williams, J. E. Schirber, D. L. Overmyer, D. Jung, J. J. Novoa, and M.-H. Whangbo, *Physica C*, **174**, 475 (1991); A. J. Schultz, M. A. Beno, U. Geiser, H. H. Wang, A. M. Kini, J. M. Williams, and M.-H. Whangbo, *J. Solid State Chem.*, **94**, 352 (1991).

56) D. Jung, M. Evain, J. J. Novoa, M.-H. Whangbo, M. A. Beno, A. M. Kini, A. J. Schultz, J. M. Williams, and P. J. Nigrey, *Inorg. Chem.*, **28**, 4516 (1989).

57) J. S. Zambounis, J. Pfeiffer, G. C. Papavassiliou, D. J. Lagouvardos, A. Terzis, C. P. Ratopoulou, P. Delhaes, L. Ducasse, N. A. Fortune, and K. Murata, *Solid State Commun.*, **95**, 211 (1995).

58) K. Oshima, T. Mori, H. Inokuchi, H. Urayama, H. Yamochi, and G. Saito, *Phys. Rev. B*, **38**, 938 (1988).

59) M. Tamura, H. Tajima, K. Yakushi, H. Kuroda, A. Kobayashi, R. Kato, and H. Kobayashi, *J. Phys. Soc. Jpn.*, **60**, 3861 (1991).

60) H. Kino and H. Fukuyama, *J. Phys. Soc. Jpn.*, **64**, 2726 (1995); **65**, 2158 (1996).

61) T. Mori, K. Oshima, and K. Kato, *Phys. Rev. B*, **51**, 11110 (1995).

62) D. B. McWhan, A. Menth, J. P. Remeika, W. F. Brinkman, and T. M. Rice, *Phys. Rev. B*, **7**, 1920 (1973); D. B. McWhan and J. P. Remeika, *Phys. Rev. B*, **2**, 3734 (1970).

63) Y. Watanabe, T. Shimizu, T. Sasaki, and N. Toyota, *Synth. Met.*, **86**, 1917 (1997).

64) P. L. Magueres, L. Ouahab, N. Conan, C. J. Gomez-Garcia, P. Delhaes, J. Even, and M. Bertault, *Solid State Commun.*, **97**, 27 (1996).

65) T. Komatsu, T. Nakamura, N. Matsukawa, H. Yamochi, G. Saito, H. Ito, T. Ishiguro, M. Kusunoki, and K. Sakaguchi, *Solid State Commun.*, **80**, 843 (1991); **82**, 101 (1992).

66) H. Urayama, H. Yamochi, G. Saito, S. Sato, A. Kawamoto, J. Tanaka, T. Mori, Y. Maruyama, and H. Inokuchi, *Chem. Lett.*, **1987**, 463.

67) U. Geiser, J. A. Schlueter, J. M. Williams, D. Naumann, and

T. Roy, *Acta Crystallogr., Sect. B*, **B51**, 789 (1995); U. Geiser, J. A. Schlueter, K. D. Carlson, J. M. Williams, H. H. Wang, W.-W. Kwok, U. Welp, J. A. Fendrich, J. D. Dudek, C. A. Achenbach, A. S. Komosa, P. M. Keane, D. Naumann, T. Roy, J. E. Schirber, W. R. Bayless, J. Ren, and M.-H. Whangbo, *Synth. Met.*, **70**, 1105 (1995).

68) J. A. Schlueter, J. M. Williams, U. Geiser, J. D. Dudek, S. A. Sirchio, M. E. Kelly, J. S. Gregar, W. H. Kwok, J. A. Fendrich, J. E. Schirber, W. R. Bayless, D. Naumann, and T. Roy, *J. Chem. Soc., Chem. Commun.*, **1995**, 1311.

69) A. M. Kini, U. Geiser, H. H. Wang, K. D. Carlson, J. M. Williams, W. K. Kwok, K. G. Vandervoort, J. M. Thompson, D. L. Stupka, D. Jung, and M.-H. Whangbo, *Inorg. Chem.*, **29**, 2555 (1990).

70) A. Kobayashi, R. Kato, H. Kobayashi, S. Moriyama, Y. Nishio, K. Kajita, and W. Sasaki, *Chem. Lett.*, **1987**, 459; R. Kato, H. Kobayashi, A. Kobayashi, S. Moriyama, Y. Nishio, K. Kajita, and W. Sasaki, *Chem. Lett.*, **1987**, 507.

71) H. Mori, I. Hirabayashi, S. Tanaka, and T. Mori, *Solid State Commun.*, **76**, 35 (1990).

72) M. Z. Aldoshina, R. N. Lyubovskaya, S. V. Konovalikhin, O. A. Dyachenko, G. V. Shilov, M. K. Makova, and R. B. Lyubovskii, *Synth. Met.*, **56**, 1905 (1993).

73) E. I. Yudanova, L. M. Makarova, S. V. Konovalikhin, O. A. Dyachenko, R. B. Lyubovskii, and R. N. Lyubovskaya, *Synth. Met.*, **79**, 201 (1996).

74) M. Fettouhi, L. Ouahab, C. Gomez-Garcia, L. Ducasse, and P. Delhaes, *Synth. Met.*, **70**, 1131 (1995).

75) E. I. Yudanova, S. K. Hoffmann, A. Graja, S. V. Konovalikhin, O. A. Dyachenko, R. B. Lubovskii, and R. N. Lyubovskaya, *Synth. Met.*, **73**, 227 (1995).

76) A. A. Galimzyanov, A. A. Ignat'ev, N. D. Kushch, V. N. Laukhin, M. K. Makova, V. A. Merzhanov, L. P. Rozenberg, R. P. Shivaeva, and E. B. Yagubskii, *Synth. Met.*, **33**, 81 (1989).

77) R. N. Lyubovskaya, E. I. Zhilyaeva, S. I. Pesotskii, R. B. Lyubovskii, L. O. Atovmyan, O. A. D'yachenko, and T. G. Takhirov, *JETP Lett.*, **46**, 188 (1987).

78) R. P. Shibaeva and L. P. Rozenberg, *Sov. Phys. Crystallogr.*, **33**, 834 (1988).

79) M. Fettouhi, L. Ouahab, D. Serhani, J.-M. Fabre, L. Ducasse, J. Amiell, R. Canet, and P. Delhaes, *J. Mater. Chem.*, **3**, 1101 (1993).

80) T. Burgin, T. Miebach, J. C. Huffman, L. K. Montgomery, J. A. Paradis, C. Rovira, M.-H. Whangbo, S. N. Magonov, S. I. Khan, C. E. Strouse, D. L. Overmyer, and J. E. Schirber, *J. Mater. Chem.*, **5**, 1659 (1995).

81) L. K. Montgomery, T. Burgin, J. C. Hoffman, K. D. Carlson, J. D. Dudek, G. A. Yaconi, L. A. Megna, P. R. Mobley, W. K. Kwok, J. M. Williams, J. E. Schirber, D. L. Overmyer, J. Ren, C. Rovira, and M.-H. Whangbo, *Synth. Met.*, **56**, 2090 (1993).

82) A. Kobayashi, T. Udagawa, H. Tomita, T. Naito, and H. Kobayashi, *Chem. Lett.*, **1993**, 2179.

83) H. Kobayashi, H. Tomita, T. Naito, A. Kobayashi, F. Sakai, T. Watanabe, and P. Cassoux, *J. Am. Chem. Soc.*, **118**, 369 (1996).

84) T. Courcet, I. Malfant, and P. Cassoux, *Synth Met.*, in press.

85) A. Kobayashi, R. Kato, T. Naito, and H. Kobayashi, *Synth. Met.*, **56**, 2078 (1993).

86) T. Komatsu, N. Matsukawa, T. Inoue, and G. Saito, *J. Phys. Soc. Jpn.*, **65**, 1340 (1996)

87) E. I. Yodanova, R. N. Lyubovskaya, R. B. Lyubovskii, S. V. Konovalikhin, and O. A. Dyachenko, *Synth. Met.*, **86**, 2195 (1997).

88) J. Wosnitza, "Fermi Surfaces of Low-Dimensional Organic Metals and Superconductors," Springer, Berlin (1996).

89) A. Kobayashi, H. Kim, Y. Sasaki, R. Kato, and H. Kobayashi, *Solid State Commun.*, **62**, 57 (1987).

90) R. Kato, A. Kobayashi, Y. Sasaki, and H. Kobayashi, *Chem. Lett.*, **1984**, 993.